Flat subduction dynamics and deformation of the South American plate: Insights from analog modeling

Nicolas Espurt,[1,2] Francesca Funiciello,[3] Joseph Martinod,[1] Benjamin Guillaume,[1] Vincent Regard,[1] Claudio Faccenna,[3] and Stéphane Brusset[1]

[1] We present lithospheric-scale analog models, investigating how the absolute plates' motion and subduction of buoyant oceanic plateaus can affect both the kinematics and the geometry of subduction, possibly resulting in the appearance of flat slab segments, and how it changes the overriding plate tectonic regime. Experiments suggest that flat subductions only occur if a large amount of a buoyant slab segment is forced into subduction by kinematic boundary conditions, part of the buoyant plateau being incorporated in the steep part of the slab to balance the negative buoyancy of the dense oceanic slab. Slab flattening is a long-term process ($\sim$10 Ma), which requires the subduction of hundreds of kilometers of buoyant plateau. The overriding plate shortening rate increases if the oceanic plateau is large enough to decrease the slab pull effect. Slab flattening increases the interplate friction force and results in migration of the shortening zone within the interior of the overriding plate. The increase of the overriding plate topography close to the trench results from (1) the buoyancy of the plate subducting at trench and (2) the overriding plate shortening. Experiments are compared to the South American active margin, where two major horizontal slab segments had formed since the Pliocene. Along the South American subduction zone, flat slab segments below Peru and central Chile/NW Argentina appeared at $\sim$7 Ma following the beginning of buoyant slab segments' subduction. In northern Ecuador and northern Chile, the process of slab flattening resulting from the Carnegie and Iquique ridges' subductions, respectively, seems to be active but not completed. The formation of flat slab segments below South America from the Pliocene may explain the deceleration of the Nazca plate trenchward velocity. **Citation:** Espurt, N., F. Funiciello, J. Martinod, B. Guillaume, V. Regard, C. Faccenna, and S. Brusset (2008), Flat subduction dynamics and deformation of the South American plate: Insights from analog modeling, *Tectonics*, *27*, TC3011, doi:10.1029/2007TC002175.

1. Introduction

[2] Flat subduction zones correspond to oceanic slabs subducting horizontally under an overriding continental plate. The best known present-day examples of flat subductions are located beneath South America, in Peru (3–15°S), and central Chile/NW Argentina (27–33°S) [e.g., *Sacks and Okada*, 1974; *Baranzangi and Isacks*, 1979; *Pilger*, 1981; *McGeary et al.*, 1985; *Cahill and Isacks*, 1992; *Engdalh et al.*, 1998; *Gutscher et al.*, 2000b; *Pardo et al.*, 2002] (Figure 1). In these two zones, the Wadati-Benioff zone and available tomographic images show the subducting plate dipping approximately 30° from the trench to a depth of 100–120 km before proceeding horizontally below the South American continental plate and sinking in the upper mantle at 700 and 600 km from the trench in Peru and NW Argentina, respectively. These two flat subduction zones are spatially correlated in the South American continental plate by (1) an absence of Quaternary volcanism as a consequence of the absence of an asthenospheric wedge between the subducting slab and the continental plate [*Nur and Ben-Avraham*, 1981; *McGeary et al.*, 1985; *Gutscher et al.*, 2000a; *Ramos et al.*, 2002; *Kay and Mpodozis*, 2002]; (2) a seismic energy released within the overriding plate larger than above the steep subduction zones, which may result from the greater contact area between the two plates [*Gutscher et al.*, 2000b; *Gutscher*, 2002]; (3) a concentration of the overriding plate shortening above the flat slab segments [*Sébrier et al.*, 1985; *Jordan and Allmendinger*, 1986; *Pardo et al.*, 2002; *Ramos et al.*, 2002; *Rousse et al.*, 2003; *Wagner et al.*, 2005; *Siame et al.*, 2005]; and (4) vertical topographic motions of the coastal areas [*Macharé and Ortlieb*, 1992; *Gutscher et al.*, 1999a; *Yañez et al.*, 2001; *Hampel*, 2002; *Clift et al.*, 2003; *Hampel et al.*, 2004b; *Wipf*, 2006], Andean Cordillera [*McNulty and Farber*, 2002], and back-arc regions on the eastern side of the Andes [*Dumont*, 1996; *Ramos et al.*, 2002; *Espurt et al.*, 2007].

[3] Two main causes have been proposed to explain the formation of these flat subduction zones:

[4] 1. The South American plate moves rapidly toward the Nazca trench in the hot spot reference frame [*Jarrard*, 1986; *Scholz and Campos*, 1995; *Silver et al.*, 1998]. Hence the active overthrusting of South America above the young Nazca oceanic plate exceeds the descent velocity of the slab

[1]Laboratoire des Mécanismes et Transferts et Géologie, Université de Toulouse, CNRS, IRD, OMP, Toulouse, France.

[2]Now at Institut Français du Pétrole, Rueil-Malmaison, France.

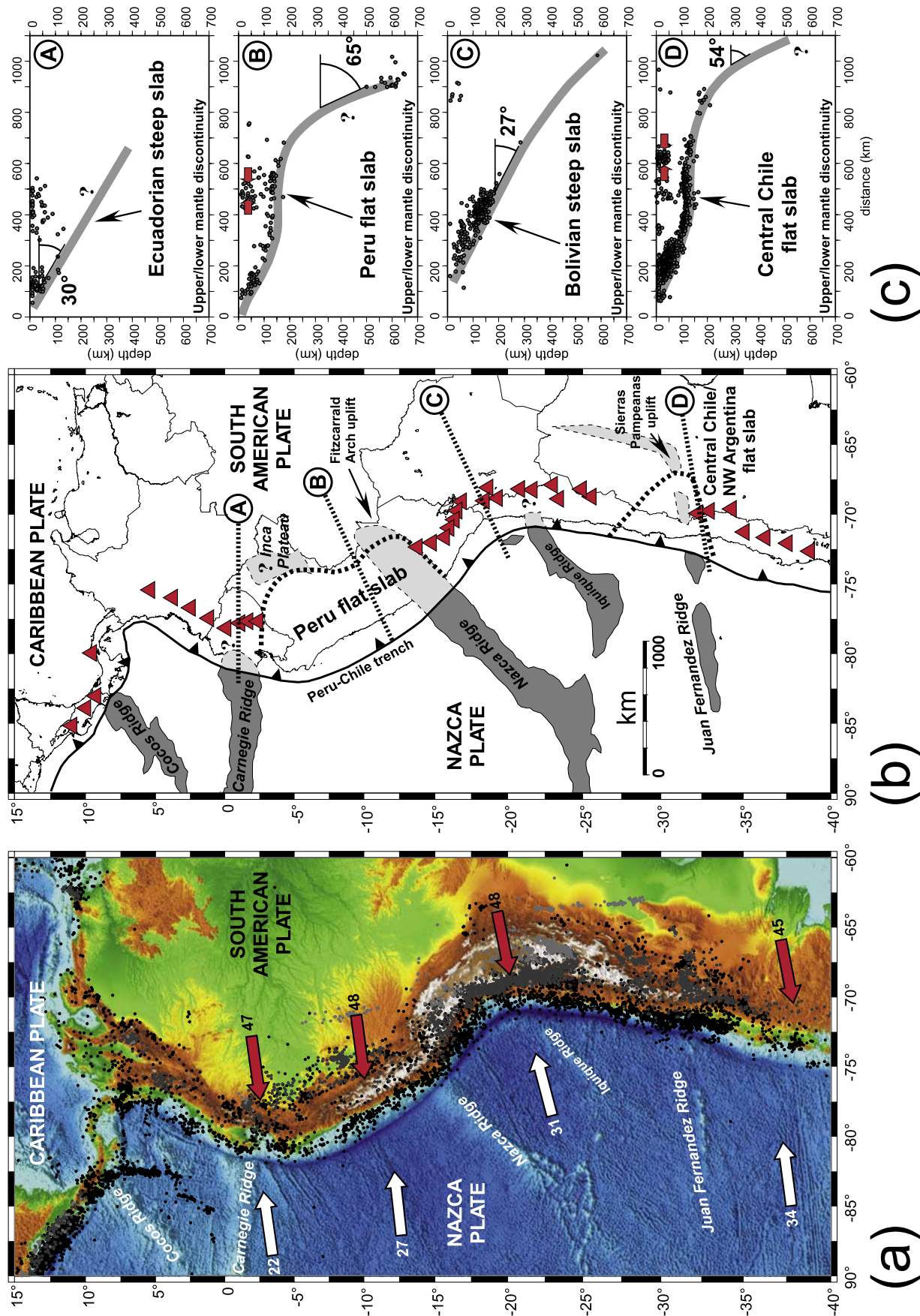[3]Dipartimento Scienze Geologiche, University Roma TRE, Rome, Italy.

Figure 1

in the upper mantle and may be responsible for the formation of flat slab segments [*Vlaar*, 1983; *van Hunen et al.*, 2002b].

[5] 2. The subduction of buoyant anomalies (such as bathymetric highs, aseismic ridges, or oceanic plateaus) increases the thickness of the crust and locally reduces the average density of the oceanic plate. Thus Peru and central Chile/NW Argentina flat subduction zones may result from buoyant oceanic segments (Nazca and Juan Fernandez ridges) taken toward subduction by global plate motion [*Nur and Ben-Avraham*, 1981; *Pilger*, 1981; *McGeary et al.*, 1985; *Gutscher et al.*, 2000b]. Other flat subduction zones reported all around the Pacific Ocean (western New Guinea, SW Japan, southern Alaska, central Mexico, and Costa Rica) suggest that parameters resulting in the formation of flat slab segments are not specific to the South American margin [*Gutscher et al.*, 2000b].

[6] Nevertheless, causes of the appearance of flat slab segments are the subject of an active discussion. For instance, it has been recently suggested that the moderate crustal thickness of the Juan Fernandez Ridge is not sufficient to make the buoyant slab responsible for horizontal subduction [*Kopp et al.*, 2004]. These authors suggest that upper mantle hydration may be an additional mechanism favoring flat subduction. In contrast, the Carnegie Ridge does not result in the formation of any flat subduction zone [*Guillier et al.*, 2001] in spite of the associated broad bathymetric anomaly (Figures 1b and 1c). The Iquique Ridge, despite having a more continuous crustal root than the Juan Fernandez Ridge, is also associated with a steeply subducting slab beneath northern Chile [*Tassara et al.*, 2006] (Figures 1b and 1c).

[7] Several kinds of analog and numerical models have been performed by previous authors to study either the conditions resulting in the occurrence of horizontal subduction zones or the consequence of the subduction of aseismic ridges on the overriding plate. Consequences of bathymetric highs and aseismic ridges' subduction on the fore-arc area have been studied by means of crustal-scale analog models using granular materials [*Dominguez et al.*, 1998; *Hampel et al.*, 2004b]. These models show that bathymetric highs and oceanic ridges have important consequences on uplift, tectonic, sedimentary, and erosional processes in the fore-arc zone. Similar observations were found using 2-D numerical models [e.g., *Chung and Kanamori*, 1978; *Kodama*, 1984; *Moretti and Ngokwey*, 1985; *Collot et al.*, 1985; *Geist et al.*, 1993]. *van Hunen et al.* [2002a, 2002b, 2004] reproduce the formation of flat slab segments resulting from the subduction of buoyant oceanic plateaus. *van Hunen et al.* [2002a, 2002b, 2004] show that the trenchward motion of the overriding plate facilitates the formation of long flat slab segments similar to those observed beneath South America. From analog experiments modeling the subduction of a viscous plate, *Martinod et al.* [2005] also conclude that flat slab segments only occur if the convergence between subducting and overriding plates is forced by external boundary conditions.

[8] The aim of this paper is to present lithospheric-scale analog models using viscous materials and to explore both the conditions permitting the appearance of flat subduction zones and their consequences on the overriding plate deformation. Experiments have been specially dedicated (1) to observe how the trenchward absolute overriding plate motion and the buoyancy of the subducting plate control the formation of a flat slab segment, (2) to study the causal and temporal relationships existing between the oceanic plateau subduction and the flattening of the slab, and (3) to study the effects of the flat subduction on the overriding plate tectonic regime. We compare our analog results with geological and geophysical data from the Andean subduction zone.

2. Model Set Up

2.1. Experimental Procedure

[9] We use Newtonian viscous materials within a Plexiglas tank ($80 \times 80 \times 20$ cm^3) to reproduce the subduction of lithospheric plates in the upper mantle (Figure 2). Lithospheric plates are modeled using high-viscosity sili-

Figure 1. Geodynamic setting of the Nazca-South American convergence system. (a) Map of the eastern Pacific Ocean and South America. Bathymetric data from the Geosat and European Remote Sensing satellite system 1 (ERS-1) spacecraft [*Smith and Sandwell*, 1997] and elevation data from NASA Shuttle Radar Topographic Mission Gtopo 30. Relative plate motions are indicated by arrows in mm a^{-1} [*Gripp and Gordon*, 2002]. These velocities are distributed asymmetrically on the Nazca and South American plates, showing a rapid westward displacement of the South American plate. Earthquake epicenters are plotted: 0–99 km in black; 100–199 km in dark gray, and 200–700 km in light gray (taken from U.S. Geological Survey (USGS) National Earthquake Information Center (USGS National Earthquake Information Center data are available at http://earthquake.usgs.gov/regional/neic/neic_bulletins.php). (b) The Nazca plate bears many topographic anomalies (aseismic ridges or oceanic plateaus marked in gray areas) where the crust is anomalous thick and buoyant. The estimated subducted lengths of these anomalies beneath the South American plate are shown in light gray areas. Red triangles mark active andesitic volcanism [*Gutscher et al.*, 2000b]. (c) Profiles of the Nazca slab beneath the South American plate from earthquake epicenters plotted [*Gutscher et al.*, 2000b]. The subduction of the Carnegie and Iquique ridges are not marked by any flat slab segment beneath northern Ecuador (marked "A") and northern Chile/Bolivia (marked "C"), respectively. In contrast, there exists a causal relationship between the subduction of the Nazca and Juan Fernandez ridges and the flat slab segments of Peru (marked "B") and central Chile/NW Argentina (marked "D"), respectively [*Gutscher et al.*, 2000b]. Red arrows show the locus of maximum shortening within the South American plate above the Peruvian and central Chile/NW Argentina flat slab segments [*Gutscher et al.*, 2000b; *Pardo et al.*, 2002].
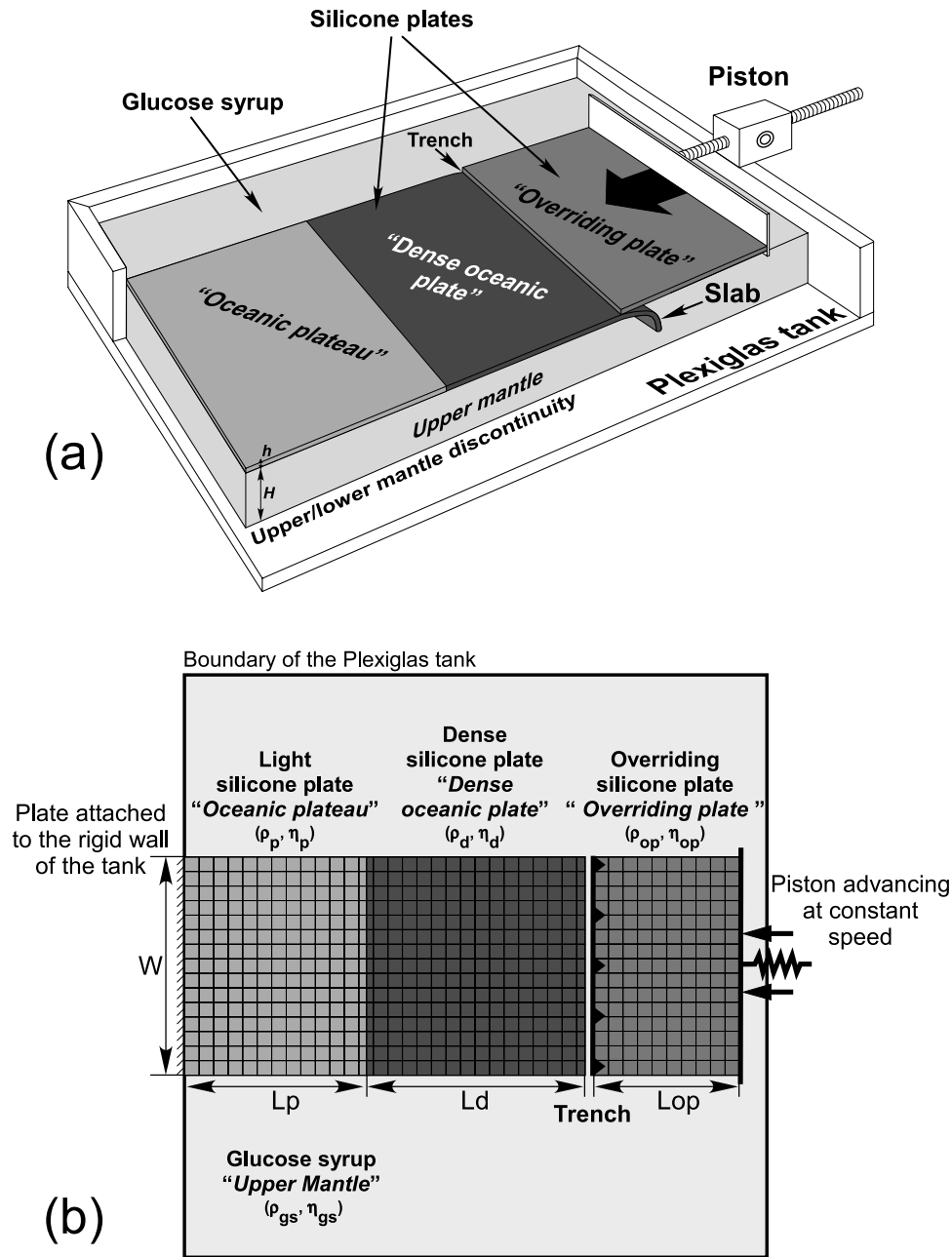
Figure 2. (a) Schematic sketch of the three-experiment set up. The silicone layers model the lithospheric plates, and the dense glucose syrup models the upper mantle. The bottom of the Plexiglas tank represents the high-gradient viscosity increase at the upper/lower mantle boundary. The subducting plate simulates a 50-Ma-old dense oceanic plate followed by a light oceanic plate (aseismic ride or oceanic plateau). See Table 3 for the values of h and H. (b) Top view of the experimental set up. Silicone plates present different densities ($\rho_{d,p,op}$) and viscosities ($\eta_{j,p,op}$) with the overriding continental plate to the right, the dense oceanic plate in the middle, and the oceanic plateau to the left. The plates are surrounded by the glucose syrup (see Table 3 for the values of ρ_{gs} and η_{gs}). An initial regular grid drawn on the overriding plate allows us to evaluate the deformation within the plates during the experiment. In the configuration drawn here, the overriding continental plate is pushed at constant speed by a piston above the subducting plate. See also Table 3 for the values of W, L_d, L_p, and L_{op}.
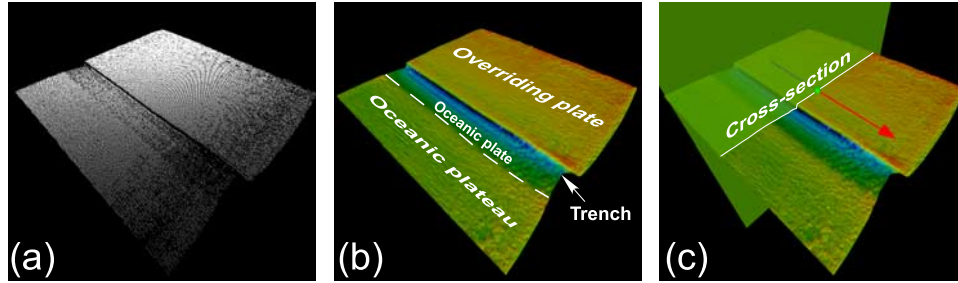
Figure 3. Perspective view of the model surface and workflow for constructing topographic cross sections. (a) Acquisition of the data with spatial coordinates *x*, *y*, and *z* by laser stereoscopic technique. (b) Surface generated from digitized points and identification of the overriding plate, oceanic plate, and the oceanic plateau. (c) Cross section plane perpendicular to the trench allowing us to see the geometrical and topographical evolution of the experiment.

cone putty. We vary the density of silicone putty to take into account the different lithosphere buoyancies. The upper mantle is modeled using a Newtonian low-viscosity glucose syrup solution. We neglect the role of thermal convection, assuming that the flow within the syrup is only generated by plate motion and slab subduction. We assume that the base of the upper mantle (bottom of the Plexiglas tank) acts as an impermeable barrier where the slab remains temporarily stalled for the adopted experimental timescales (Figure 2a) [*Funiciello et al.*, 2003]. The system is isothermal, which implies that the density contrast between the lithosphere and the upper mantle is only chemically implemented and kept constant during the entire evolution of the experiment (see the paper by *Funiciello et al.* [2003] for more details on the experimental procedure).

[10] Silicone plates that represent the subducting and overriding plates, respectively, initially float above the dense glucose syrup (Figure 2b). The lateral distance between plates and the sides of the Plexiglas tank containing the experiment is larger than the size of advected cells within the upper mantle to minimize lateral boundary effects. Thus we assume that lithospheric plates are completely surrounded by weak fault zones [*Funiciello et al.*, 2004]. We take into account neither lateral heterogeneities within the plates nor the oblique plate convergence. During the subduction, the overriding and subducting plates are separated by a thin layer of glucose syrup at trench. Hence we assume that the subduction fault plane is weak, with the same viscosity as in the upper mantle. Moreover, we always lubricate the complete surface of the subducting plate with Vaseline, so as to avoid plates sticking. In the initial configuration, the leading edge of the silicone plate is forced downward to a depth of 3 cm (corresponding to about 200 km in nature) inside the glucose syrup to initiate the subduction process. In experiments 1−3 (Table 3), the subduction velocity is not imposed by kinematic boundary conditions but only results from the negative buoyancy of the subducting slab (i.e., slab pull) [*Funiciello et al.*, 2003]. In contrast, in experiments 4−8 (Table 3), a constant convergence rate between subducting and overriding plates is imposed, advancing a rigid piston perpendicular to the trench (Figure 2a). The piston is plunged into the upper part

of the glucose syrup at a depth of 18 mm, and the syrup is free to move underneath. It pushes the overriding plate toward the trench. A regular grid initially drawn on the overriding plate allows us to measure the finite displacement field of each single node of the grid along the *x* and *y* directions at each time interval (Figure 2b). The cumulative deformation of each element of the grid during the experiment is then calculated, integrating the finite displacement field over the time. Experiments are monitored with lateral and top view photos, and the topography of some selected experiments has been monitored with a topography scanner (Real Scan USB model 300) (Figure 3).

2.2. Similarity Criteria

[11] Experimental parameters and scaling relationships for the reference experiment (experiment 1) are listed in Tables 2 and 3, respectively. Materials have been selected to respect the standard scaling procedure for length, density, viscosity, and stress in a natural gravity field ($g_{Model} = g_{Nature}$) as described by *Weijermars and Schmeling* [1986] and *Davy and Cobbold* [1991].

[12] The scale factor for length is 1.5×10^{-7}, i.e., 1 cm in the experiment corresponds to ∼66 km in nature. We model the subduction of wide and homogenous buoyant plates assuming that (1) the Inca Plateau and the Nazca Ridge form a 1500-km-wide buoyant anomaly [*Gutscher et al.*, 1999b] and (2) the Juan Fernandez Ridge was oriented nearly parallel to the trench in the Lower Miocene [*Yañez et al.*, 2001] (Figure 1b). In nature, aseismic ridges or oceanic plateaus correspond to topographic anomalies where the crust is thicker than the surrounding oceanic plate, increasing the buoyancy of the oceanic lithosphere [*Cloos*, 1993; *Molnar and Gray*, 1979]. In our simplified models, we consider that the thickness of the lithosphere below aseismic ridges or oceanic plateaus is similar. The density of silicone plates is scaled to simulate the average density of the corresponding natural lithospheric plates (Table 2), and we reduce the density of the silicone lithospheric plate over its whole thickness. Such an approximation should not modify the general behavior of the subduction zone, assuming that the oceanic crust is not delaminated from the mantle during the process of subduction [*Chemenda et al.*,

2000]. In the reference experiment (experiment 1), the buoyancy of the silicone plate modeling the dense oceanic plate is $(\Delta\rho_d)_{Model} = -80$ kg m^{-3}, whereas the buoyancy of the plate modeling the plateau-bearing oceanic lithosphere is $(\Delta\rho_l)_{Model} = +41$ kg m^{-3} (Table 2). If we consider that we model a 50-Ma-old dense oceanic lithosphere (maximum age of the Nazca slab between 10 and 35°S) whose negative buoyancy is $(\Delta\rho_l)_{Nature} = -35$ kg m^{-3} [*Cloos*, 1993], the adopted buoyancy-scaling factor is $(\Delta\rho_l)_{Model}/(\Delta\rho_l)_{Nature} = 2.3$. Thus the buoyancy of the plateau-bearing oceanic lithosphere corresponding to the light silicone plate in nature is $(\Delta\rho_l)_{Nature} = +18$ kg m^{-3}, which corresponds to a 50-Myr-old oceanic lithosphere with a 17-km-thick crust. Such a plateau would result in a ∼1900-m-high bathymetric anomaly, similar to that of the Nazca Ridge (see the paper by *Martinod et al.* [2005] for further details concerning the scaling of buoyant anomalies).

[13] The ratio of the oceanic lithosphere viscosity over the upper mantle viscosity is set to an upper bound of roughly 10^4. From the simple scaling equations of Table 2, we find that 1 min corresponds to 1.4 Ma in nature.

3. Experimental Results

[14] Eight models have been performed using various combinations of geometrical, kinematical, and rheological parameters, with the aim to explore the subduction of a negatively buoyant oceanic plate, followed by the subduction of a buoyant plate modeling a wide oceanic plateau with or without an upper overriding plate (Figure 2 and Table 3). The evolution of three selected experiments is described in sections 3.1, 3.2, and 3.3 (experiments 1, 4, and 8 (Table 3)).

3.1. Subduction of a Plateau Below a Free Overriding Plate (Reference Experiment, Experiment 1 (Table 3))

[15] Experiment 1 shows the subduction of a fixed oceanic lithosphere followed by a light oceanic plateau beneath an overriding plate being free to move above the subduction zone (Figure 4a). *Martinod et al.* [2005] have already described the behavior of a similar experiment without any upper overriding plate (e.g., experiments 2 and 3 in Table 3). Our experiment shows the typical sequence of events already described by *Martinod et al.* [2005], i.e., subduction initiation and slab interaction with the base of the upper/lower mantle discontinuity followed by a steady state regime of subduction of the dense part of the slab (Figures 4a and 4b). During the steady state regime and as far as the dense part of the plate is concerned, subduction is characterized by a velocity of subduction of 0.3 mm s^{-1} and a dip of 53°, as in the paper by *Martinod et al.* [2005]. As soon as the buoyant plateau starts subducting, the velocity of subduction suddenly decreases, and the slab steepens (Figures 4a, 4b, and 4c). Finally, the process can be stopped when ∼4 cm of the buoyant plateau (corresponding to ∼280 km in nature) have been subducted, enhancing the progressive verticalization of the slab (Figure 4a). During the whole experiment, the overriding plate passively follows the retreating trench (Figure 4a) and does not deform.

3.2. Subduction of a Plateau Below a Pushed Overriding Plate (Experiment 4 (Table 3))

[16] In experiment 4, the overriding plate is pushed at a constant velocity of 0.31 mm s^{-1} by a piston, moving perpendicularly toward the trench (Figure 5a). All the other parameters are similar to those of the reference experiment (experiment 1). The subducting plate being fixed, the trench velocity is the velocity of subduction (Figure 5b). In this experiment, we observe that a fraction of the velocity imposed by the piston is accommodated by the horizontal shortening of the overriding plate, and the difference between the piston velocity and trench velocity is the overriding plate shortening rate (Figures 5b and 5d). However, the deformation of the overriding plate being slow compared to the speed of the piston, the trench motion and the velocity of subduction are essentially constrained by the advance of the piston (Figure 5b).

[17] During the subduction of the dense oceanic plate, the dip of the slab is shallower (∼49°) (Figures 5a and 5c) than in the reference experiment because of the forced advancing of the overriding plate toward the incoming plate. The plateau reaches the trench after ∼14 min of run. Initially, plateau subduction initiates without any major change in the slab geometry (Figures 5a and 5c). When ∼5.5 cm of plateau have been subducted and the tip of the plateau has reached a depth of ∼4 cm, the slab geometry reorganizes into two dip domains: The upper part becomes shallower, while the lower part of the slab steepens to 57° (Figures 5a, 5c, and 6a). Seven minutes later (∼10 Ma in nature), i.e., when 11 cm of plateau have subducted (∼730 km in nature), the plateau directly underplates the overriding plate, and a flat slab segment occurs. During this phase, the slab geometry presents three inflection points, showing that it is easier to fold and unfold the slab to maintain the plateau below the overriding plate than to increase the depth of the plateau in the inclined segment (Figures 5a, 5c, and 6a). The tip of the plateau is stabilized in the steep part of the slab at a depth of roughly 7 cm (∼460 km). Until the end of the experiment, the length of the horizontal slab segment increases to finally reach a length of 4.2 cm, the edge of the flat slab segment being located at 8.9 cm from the trench (corresponding to ∼620 km in nature).

[18] During the subduction of the dense oceanic plate, the overriding plate shortening is close to zero (Figures 5d and 7) because the imposed convergence velocity is close to the velocity of subduction in the corresponding free subduction experiment (reference experiment). The advance of the overriding plate forces the subduction of the plateau, but the overriding plate shortening starts with a delay of about 2 min (Figure 5d). The overriding plate shortening of ∼4.5 × 10^{-4} s^{-1} shows that the process of subduction is now opposed by the slab buoyancy. It results in a decrease of the velocity of subduction (from 0.31 to 0.24 mm s^{-1}) (Figures 5b and 5d). Before the formation of the flat slab segment, the overriding plate homogeneously shortens, except close to the trench where the slab and the overriding plate touch closely (Figure 7). In this area (that would correspond to the fore-arc region in nature), the force exerted by the slab results in a trenchward decrease of the
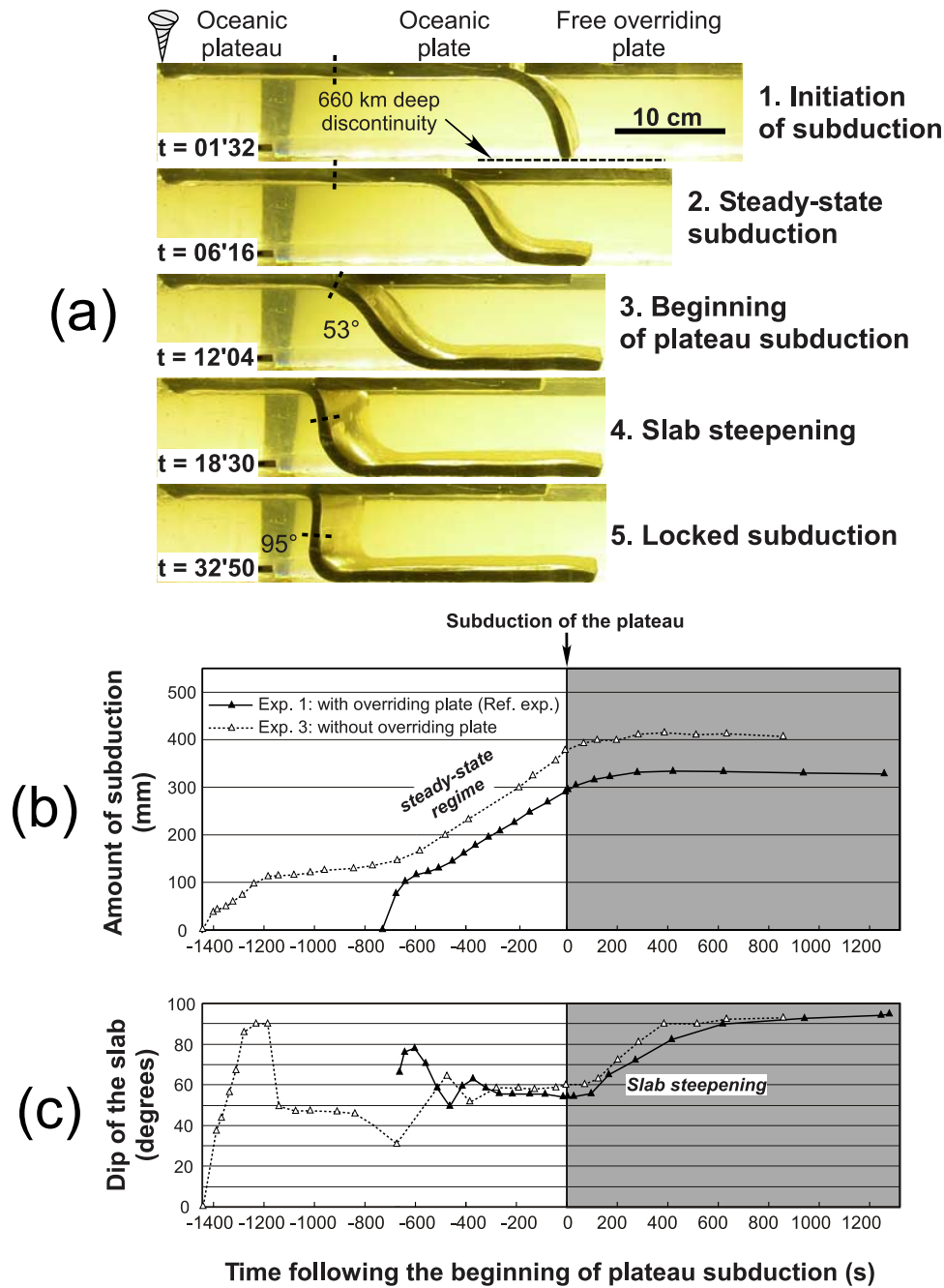
Figure 4. Experiment 1. (a) Lateral views of the experiment. The dashed line marks the tip of the oceanic plateau. The numbering scheme is as follows: (1) $t = 01'32$ (the slab interacts with the bottom of the box), (2) $t = 06'16$ and $12'04$ (steady state subduction pursues at constant speed, and the slab dip maintains a constant value of $53°$ until the beginning of plateau subduction), (3) $t = 06'16$ and $12'04$ (steady state subduction pursues at constant speed, and the slab dip maintains a constant value of $53°$ until the beginning of plateau subduction), (4) $t = 18'30$ (the oceanic plateau entered in subduction, decreasing the velocity of subduction and increasing the dip of the slab), and (5) $t = 32'50$ (the buoyancy of the oceanic plateau stops the subduction process). (b) Amount of subduction and (c) dip of the slab versus time. Results of experiment 3 realized without any overriding plate are shown for comparison (dashed lines with white triangles).
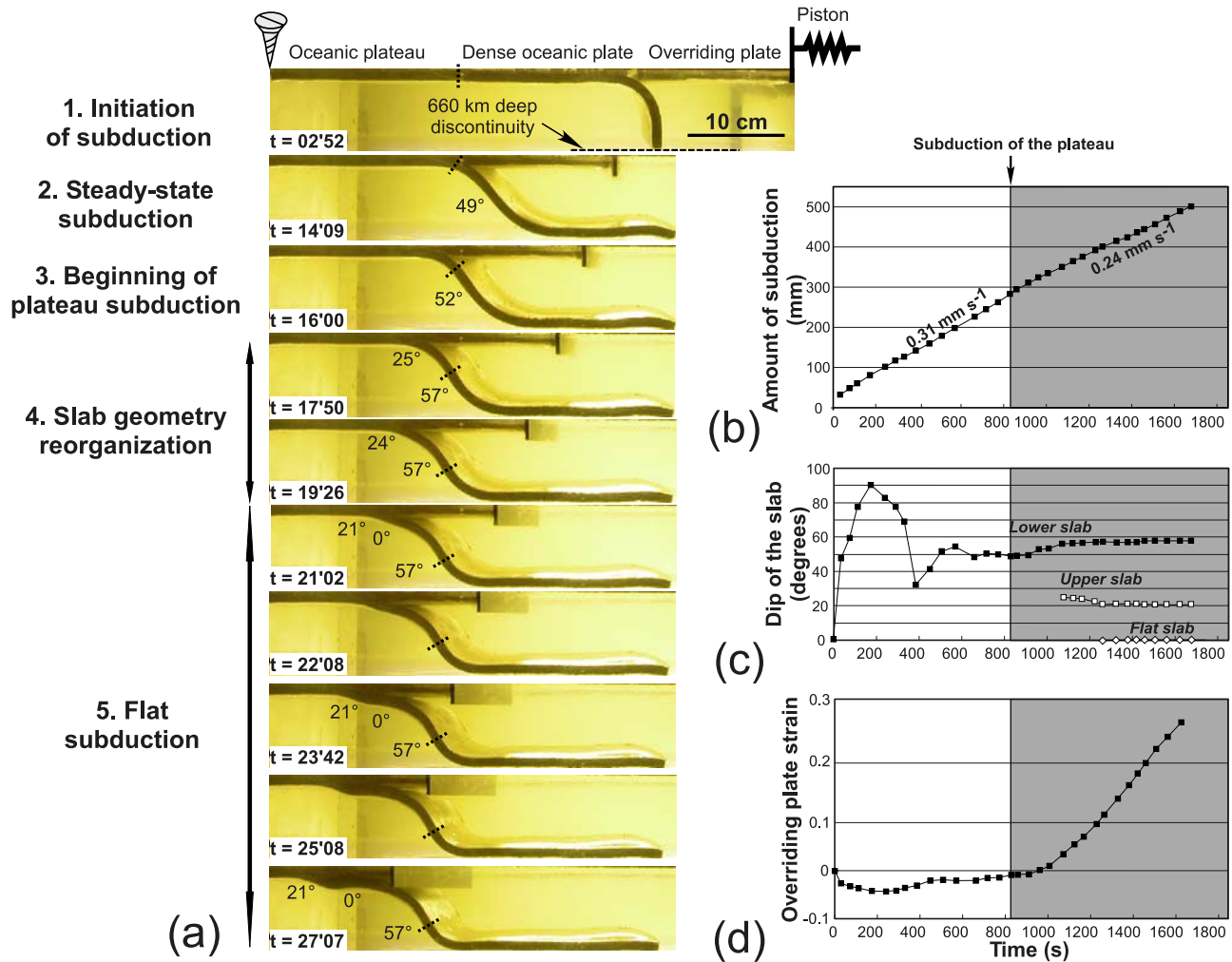
Figure 5. Experiment 4. (a) Lateral views of the experiment. The dashed line marks the tip of the oceanic plateau. The numbering scheme is as follows: (1) $t = 2'52$ (initiation of subduction), (2) $t = 14'19$ (steady state dense oceanic subduction with a constant dip of 49°), (3) $t = 16'00$ (subduction of the plateau without any perturbation in the subduction process), (4) $t = 17'50$ and $19'26$ (the plateau buoyancy perturbs the subduction process, i.e., the dip of the upper part of the slab decreases, but the dip of the lower part of the slab increases), and (5) $t = 21'02$ to $27'07$. (For $t = 21'02$ to $27'07$, the oceanic plateau flattens and underplates the overriding plate. Note that the flat slab segment is shorter than the length of the subducted oceanic plateau.) (b) Amount of subduction, (c) dip of the slab, and (d) overriding plate strain versus time.

horizontal compressive stress within the overriding plate [*Dalmayrac and Molnar*, 1981], explaining why the plate shortening is smaller there (Figure 7). When the plateau underplates the overriding plate, the contact between converging plates progressively spreads out. The locus of maximum overriding plate shortening is above the termination of the flat slab segment and progressively migrates within the overriding plate as the flat slab segment broadens (Figure 7). The shortening rate of the inner part of the overriding plate (close to the piston) also increases, because the wider contact between the converging plates results in larger friction forces between them.

[19] Laser data of Figure 8 register the evolution of the overriding plate topography and location of vertical displacements during the experiment. During the subduction of the dense plate, the continent does not present any vertical displacement. In contrast, the overriding plate topography is strongly affected by the plateau subduction. Uplift of the overriding plate close to the trench occurs as soon as the plateau subducts, despite the fact that the overriding plate shortening has not begun (Figures 5d, 8a, and 8b). Afterwards, the uplift of the overriding plate continues at a constant and slower speed until the end of the experiment, and the uplifted area spreads out within the overriding plate (back-arc region) (Figures 8a and 8b).
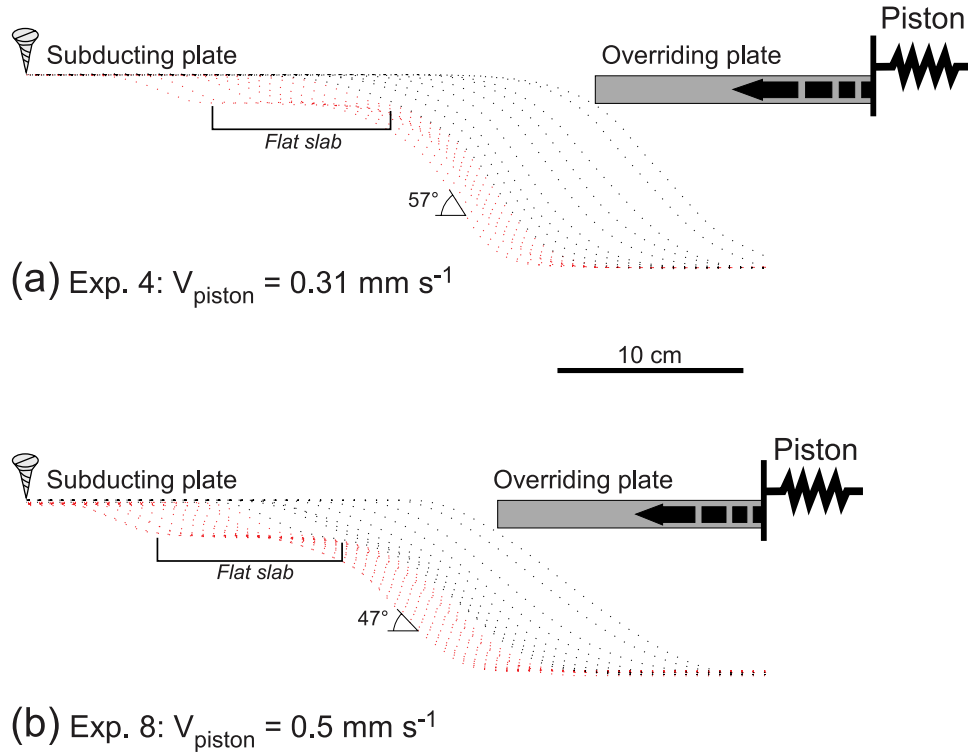
Figure 6. Kinematic behavior of the slab (dotted lines) in (a) experiment 4 and (b) experiment 8 with different piston velocities. Flat subduction episode is in red.

3.3. Subduction of a Plateau Below a Faster Overriding Plate (Experiment 8 (Table 3))

[20] In experiment 8, the piston velocity is larger than in the previous experiment (0.5 mm s^{-1} versus 0.31 mm s^{-1} in experiment 4). The higher trenchward overriding plate velocity results in a decrease of the slab dip during the

steady state subduction of the dense oceanic plate (39° versus 49° in experiment 4 (Figures 9a and 9c)). Following plateau subduction, the larger convergence velocity induces the rapid formation (4 min later, i.e., ~7 Ma in nature) of a flat slab segment (Figures 9a and 9c). As in experiment 4, the flat slab segment required ~11 cm of plateau subduction
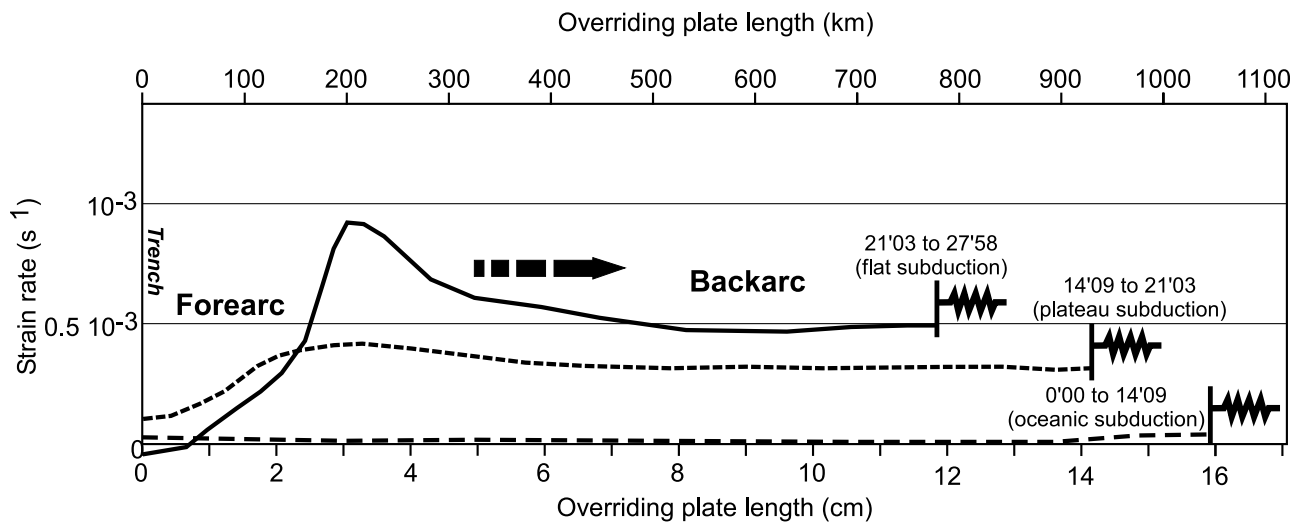

Figure 7. Overriding plate strain rate fields parallel to the convergence direction in experiment 4 during the subduction of the dense ocean (dashed line), the beginning of plateau subduction (dotted line), and flat slab subduction (solid line).
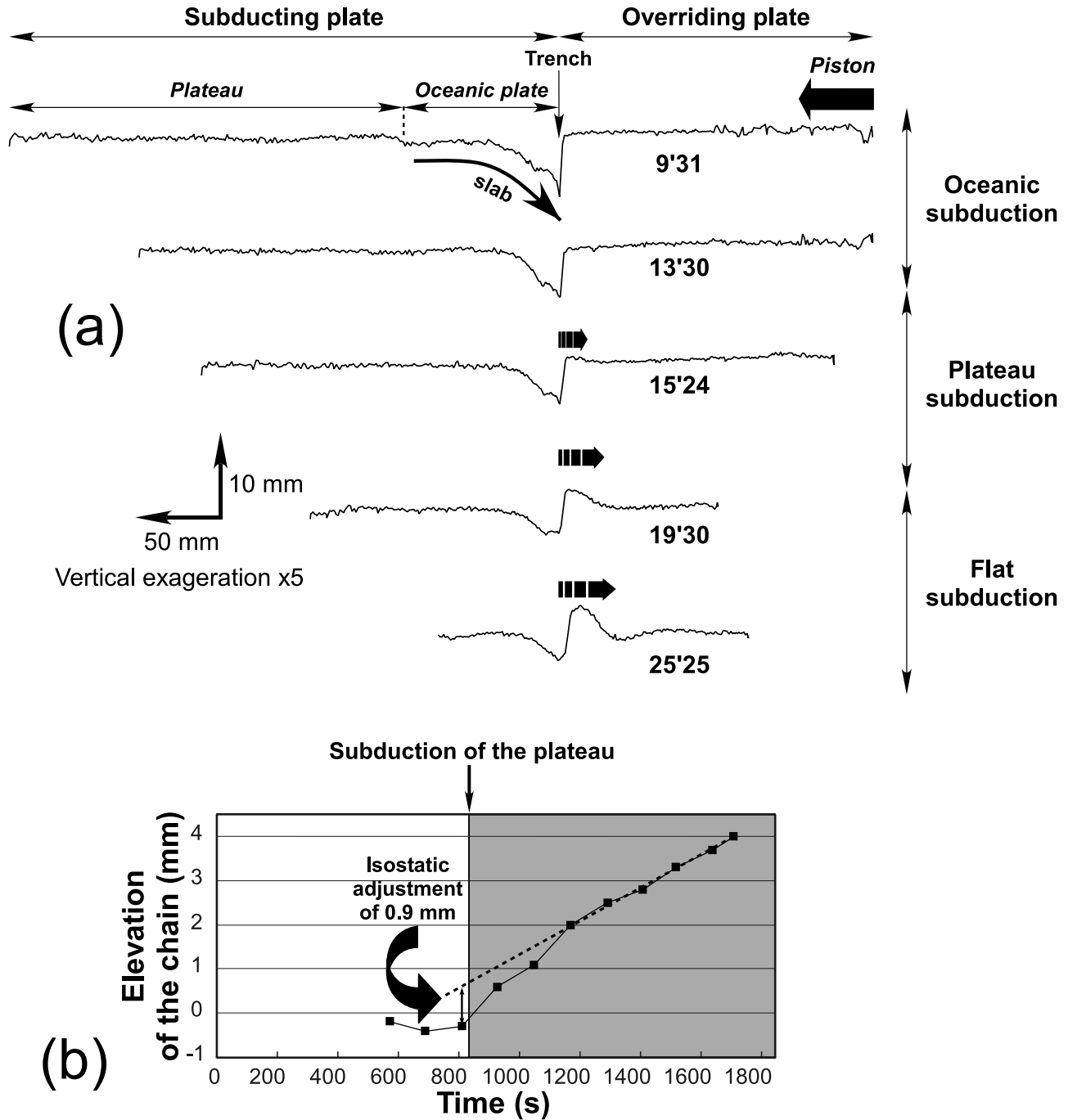
Figure 8. (a) Cross sections of experiment 4 along the centerline of the overriding plate at different times showing the propagation of the deformation within the overriding plate in response to the plateau subduction. (b) Maximum elevation of the overriding plate topography versus time. See section 4.3 for further explanations.

to occur, and the formation of the flat slab segment is marked by an increase of the dip of the lower part of the slab, here from 39° to 48° (Figures 9a and 9c). Here, again, the tip of the plateau stabilizes within the steep part of the slab at a depth of ~7 cm.

[21] In this experiment, the shortening of the overriding plate starts as soon as the tip of the dense slab touches the bottom of the tank (Figures 9b and 9d). The higher convergence velocity results in a compressional regime in the overriding plate during the steady state subduction of the
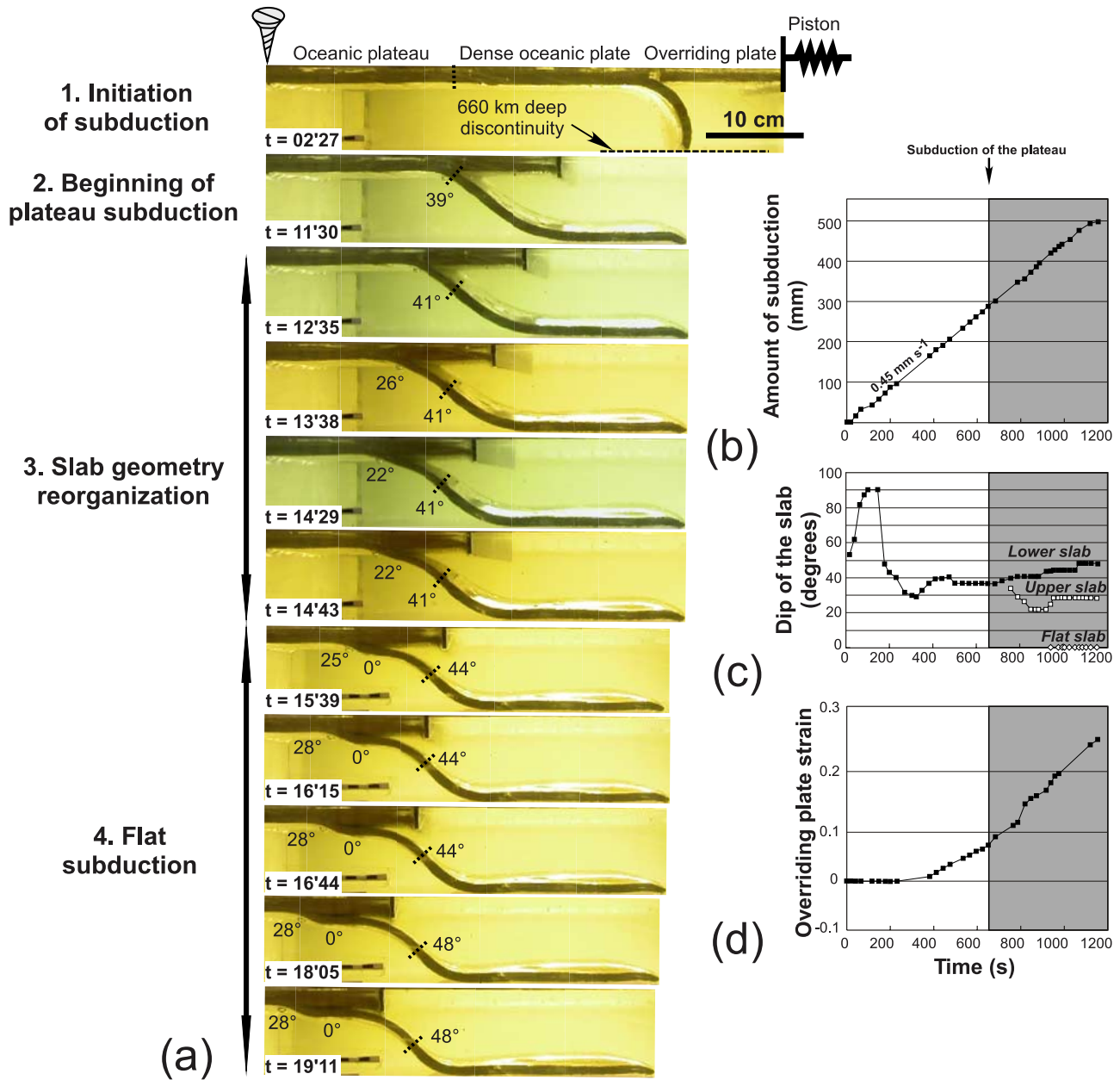
Figure 9. Experiment 8. (a) Lateral views of the experiment. The dashed line marks the tip of the oceanic plateau. The numbering scheme is as follows: (1) $t = 2'27$ (initiation of subduction), (2) $t = 11'30$ (steady state subduction of the dense oceanic subduction with a constant dip of 39°), (3) $t = 12'35$ to $14'43$ (plateau subduction without any perturbation in the subduction process), and (4) $t = 15'35$ to $19'11$ (slab flattening and formation of a horizontal slab segment). (b) Amount of subduction, (c) dip of the slab, and (d) overriding plate strain versus time.

dense plate, its shortening rate being approximately 2.3×10^{-4} s^{-1}. Following plateau subduction, the shortening rate of the overriding plate increases to ~4.5×10^{-4} s^{-1} (Figure 9b). As in experiment 4, three domains with different strain regimes occur in the overriding plate, following the occurrence of flat subduction: (1) The deformation is small close to the trench where the overriding and subducting plates touch closely, (2) the shortening is maximum above the termination of the flat slab segment, and

(3) the shortening is moderate in the rest of the overriding plate far from the trench.

4. Interpretation and Discussion: Insights on the Andean Subduction Zone

[22] The three lithospheric-scale analog experiments described in sections 3.1, 3.2, and 3.3 have been selected to
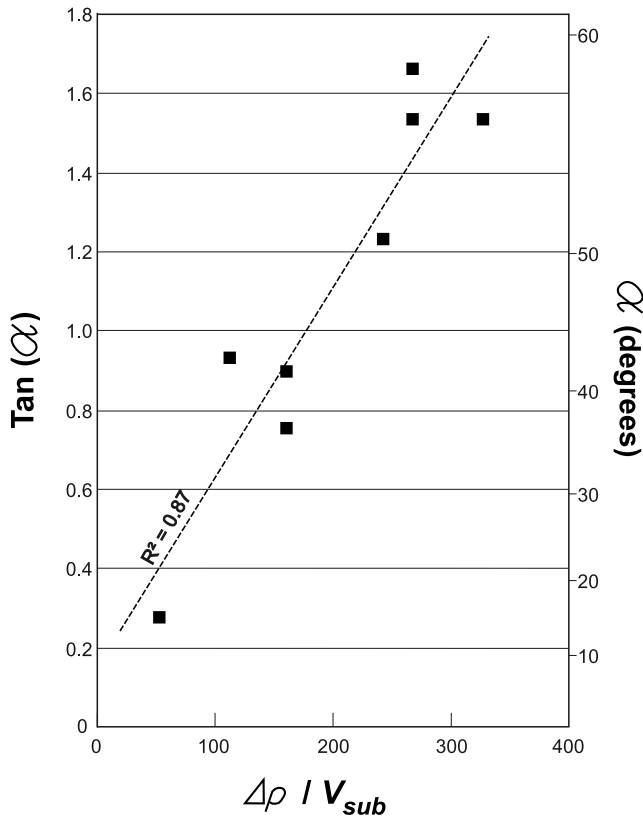
Figure 10. Dip of the slab (α) versus $\Delta\rho/V_{sub}$ in experiments 1–8 (see Table 3), where $\Delta\rho$ is the negative buoyancy of the subducting plate, and V_{sub} is the velocity of subduction. The linear relationship between $\Delta\rho/V_{sub}$ and $\tan(\alpha)$ shows that the vertical component of the slab velocity does not depend on the overriding plate motion in this set of experiments.

show the evolution of the slab geometry as a function of the overriding plate motion and subducting plate buoyancy. In sections 4.1, 4.2, and 4.3, we show how their evolution gives insights to understand processes resulting in flat subductions beneath the Andes and the large-scale associated tectonic processes within the overriding South American plate.

4.1. Parameters Controlling the Flat Subduction

[23] Experimental results confirm that the subduction of a buoyant lithosphere (such as an oceanic plateau) is not the only element that results in the formation of a flat slab segment [*Martinod et al.*, 2005]. Experiment 1 shows that part of subducted buoyant plateaus can easily sink in the upper mantle and be incorporated in the steep lower part of the slab (Figure 4a). The buoyancy of the plateau is compensated by the negative buoyancy of the dense oceanic slab. If the overriding plate is free to move, the dip of the slab increases following plateau subduction as the velocity of subduction decreases [*Bellahsen et al.*, 2003; *Martinod et al.*, 2005]. Flat subduction cannot occur, and the buoyant

anomaly stops the process of subduction, producing a slab verticalization (Figure 4a). Although the average buoyancy of the slab is still slightly negative at the end of experiment 1, its magnitude is too small to maintain the subduction active [*Martinod et al.*, 2005]. In natural cases, plateau subduction decreases subduction velocity, and simultaneous slab steepening may be followed by slab break-off (see the papers by *Regard et al.* [2005] and *Conrad et al.* [2004] and Mediterranean examples described by *Wortel and Spakman* [2000], for instance). However, the simplified Newtonian viscous rheology adopted to simulate the experimental lithosphere does not favor the occurrence of this phenomenon in our models.

[24] So far, we have only considered the specific case in which plates' motion only results from forces acting in the subduction zone (slab pull force). However, in nature, the absolute motion of lithospheric plates can be also influenced by global far-field boundary conditions that are able to partly control the velocity of subduction. For example, the rapid westward motion of the South American lithosphere above the Nazca plate [*Marrett and Strecker*, 2000] seems to be controlled by the opening of the Atlantic Ocean and the motion of Africa [*Silver et al.*, 1998].

[25] Our experimental results suggest that the trench migration imposed by the trenchward motion of the overriding plate does not modify the vertical component of slab velocity. In the entire experimental set (see Table 3) and during the steady state subduction of the dense oceanic plate, we observe that $V_z = V_{sub} \tan(\alpha)$ is proportional to $\Delta\rho$, where V_{sub} is the velocity of subduction, V_z the vertical component of the slab velocity, α the dip of the slab, and $\Delta\rho$ the slab buoyancy (see Figure 10). Hence experimental results suggest that the appearance of flat slab segments cannot be produced even if we increase the overriding plate trenchward velocity as long as the slab is negatively buoyant, since the vertical component of the slab velocity is maintained independently of trench motion. *Heuret et al.* [2007] also observed that plate kinematics can strongly affect the evolution of the subduction process. In particular, they noted that the motion of the overriding plate toward the trench enhances trench rollback and slab shallowing, despite the fact that the subducted lithosphere is dense and heavy [*Scholz and Campos*, 1995; *Heuret et al.*, 2007]. However, the dense slab can never reach a dip inferior to 18°, even if it is strongly forced to subduct [*Heuret et al.*, 2007].

[26] In fact, our experiments suggest that the presence of a buoyant subducting plateau and an overriding plate pushed toward the trench by lateral boundary conditions are necessary for flat slab segments to occur (experiments 4 and 8) (Figure 6). For instance, the buoyant effect of the Inca Plateau and Nazca Ridge subduction beneath the trenchward advancing of South America plate would be responsible for the 1500-km-wide Peruvian flat slab segment [*Gutscher et al.*, 1999b]. In southern South America, the Juan Fernandez Ridge coincides with the central Chile/NW Argentina flat slab segment [*Pilger*, 1981]. In these two zones, the present-day flat slab segments are clearly illustrated by seismicity data (Figure 1c) [*Gutscher et al.*, 2000b; *Pardo et al.*, 2002]. Earthquakes at ∼120-km depth show

Table 1. Ridge/Plateau Subduction Characteristics Along the Andean Subduction Zone

Ridge/ Plateau	Width (km)	Height (km)	Crustal Thickness (km)	Origin	Symmetric on Pacific Plate	Beginning of Subduction (Ma)	Length of Subduction (km)	Flat Slab Segment	Upper Plate Uplift
Carnegie[a]	280	2	13–19	Galapagos hot spot	-	1	~70(?)	no	yes (only fore arc)
Inca[b]	~300	-	-	Pacific spreading ridge hot spot	Marquesas plateau	13	~900(?)	yes	no
Nazca[c]	200	1.5	18 ± 3	Pacific spreading ridge hot spot	Tuamotu plateau	11.2	~900	yes	yes
Iquique[d]	130	1.5	15	Pacific spreading ridge hot spot	Austral plateau	2	~150(?)	no	no
J. Fernandez[e]	<100	4	15	hot spot located near the Alejandro Selkirk island	-	12	~850	yes	yes

[a][*Lonsdale and Klitgord*, 1978; *De Vries*, 1988; *Deniaud et al.*, 1999; *Gutscher et al.*, 1999a; *Guillier et al.*, 2001; *Spikings et al.*, 2001; *Sallarès et al.*, 2005; *Pedoja et al.*, 2006].

[b][*Gutscher et al.*, 1999b].

[c][*Soler and Bonhomme*, 1990; *Dumont*, 1996; *Hsu*, 1992; *Macharé and Ortlieb*, 1992; *Gutscher et al.*, 1999b; *Woods and Okal*, 1994; *Le Roux et al.*, 2000; *Latrubesse and Rancy*, 2000; *McNulty and Farber*, 2002; *Hampel*, 2002; *Rousse et al.*, 2003; *Hampel et al.*, 2004a, 2004b; *Rosenbaum et al.*, 2005; *Tassara et al.*, 2006; *Espurt et al.*, 2007].

[d][*Gutscher et al.*, 1999b; *Rosenbaum et al.*, 2005; *Tassara et al.*, 2006].

[e][*Allmendinger et al.*, 1983; *Jordan and Alonso*, 1987; *Reynolds et al.*, 1990; *von Huene et al.*, 1996; *Pardo et al.*, 2002; *Ramos et al.*, 2002; *Kopp et al.*, 2004; *Tassara et al.*, 2006; *Farias et al.*, 2008].

the flat slab segments advancing beneath the overriding plates at more than 600 km east of the trench. In contrast, the eastern intermediate slab (between 200 and 600 km) is steeper (~60°) than elsewhere beneath South America (~30°). The slab flattening is accompanied by an increase of the dip of the intermediate part of the slab, as observed in experiments 4 and 8 (Figure 6).

[27] *Kopp et al.* [2004] recently found that the Juan Fernandez Ridge may not have sufficient buoyancy to generate a flat slab segment. The Juan Fernandez Ridge is a discontinuous topographic anomaly ~4 times smaller than the Nazca Ridge (see Figure 1a and Table 1). *Kopp et al.* [2004] suggest that upper mantle hydration along ridge-parallel fault zones decreases the density of the oceanic plate and consequently favors the buoyancy of the slab. In fact, the reconstruction of the Juan Fernandez Ridge geometry suggests a 20°N ridge segment (i.e., almost trench parallel), which subducted below northern Chile between 25 and 12 Ma [*Yañez et al.*, 2001]. The effect of trench-parallel buoyant anomalies on the dynamics of subduction is significantly larger than the effect of trench-perpendicular ridges [see *Martinod et al.*, 2005]. Thus this ridge segment may also explain the formation of the central Chile/NW Argentina flat slab segment in spite of the modest size of the Juan Fernandez Ridge. In the absence of any symmetric of the Juan Fernandez Ridge on the Pacific plate, it is impossible to evaluate the volume of the ridge segment that subducted since the Lower Miocene below Chile. Despite the fact that the volume of the Juan Fernandez Ridge segment now visible in the Pacific seafloor is modest (see Figure 1a), the volume of magma that resulted from the Juan Fernandez hot spot activity (Table 1) in the past may

have been larger. Thus we do not think it is necessary to involve upper mantle hydration to explain the central Chile/ NW Argentina flat subduction zone, although this phenomenon may undeniably result in lighter oceanic lithosphere [*Kopp et al.*, 2004].

4.2. Timing of the Flat Subduction

[28] The appearance of a flat slab segment is a process that initiates after several Ma following the beginning of plateau subduction (experiment 4). This delay decreases when the overriding plate velocity increases (experiment 8). In fact, experiments show that slab flattening requires time to occur because at the beginning of plateau subduction its buoyancy is compensated by the negative buoyancy of the lower part of the slab (Figures 11 and 12). We observe that flat subduction occurs when the average buoyancy of the inclined part of the slab turns positive. The delay between the beginning of plateau subduction and the formation of a flat slab segment has also been observed by *van Hunen et al.* [2002a, 2002b] (Figure 11). The delay is larger in our experimental set, probably because the numerical setup of *van Hunen et al.* [2002a, 2002b] does not take into account the negative buoyancy of the slab below 400-km depth.

[29] The Nazca Ridge subduction beneath the Peruvian coast started ~11.2 Ma ago [*Hampel*, 2002], and the volcanism has been inactive above the ridge segment since ~4 Ma, in response to the flattening of the slab (Figure 12) [*Soler and Bonhomme*, 1990; *Rosenbaum et al.*, 2005; *Espurt et al.*, 2007]. *Yañez et al.* [2001] showed that near 30°S, the Juan Fernandez Ridge subduction started approximately 12 Ma ago. Its subduction is followed by the end of
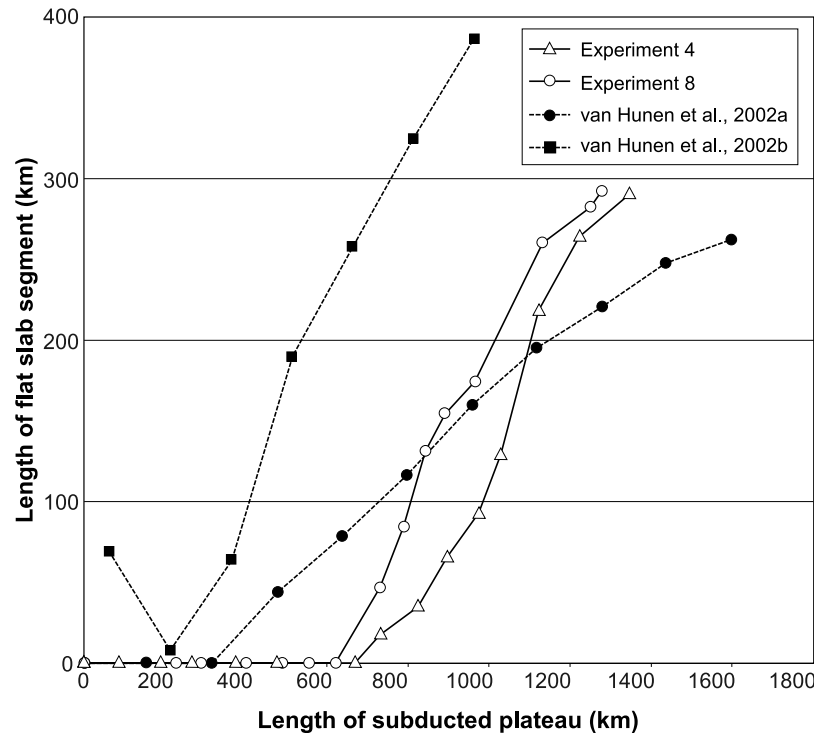
Figure 11. Length of the flat slab segment versus length of subducted plateau in experiments 4 and 8. Numerical results without overriding plate motion [*van Hunen et al.*, 2002a] and with overriding plate motion [*van Hunen et al.*, 2002b] are shown for comparison.

the arc volcanism at ~5 Ma [*Ramos et al.*, 2002]. Thus the delay between the subduction of the buoyant anomalies and the appearance of the two present-day flat slab segments below South America is ~7 Ma, which is equivalent to the delay observed in the experiments (Figure 12). It may also explain why broader ridges such as the Carnegie or Iquique ridges do not result in the formation of any modern flat subduction zone. For *Lonsdale and Klitgord* [1978], the Carnegie Ridge subduction only began 1 Ma ago. The analysis of seismicity distribution suggests that the slab plunges below northern Ecuador with a dip close to 30° down to a depth of at least 200 km [*Guillier et al.*, 2001] (Figure 1c). In fact, the broadening of the volcanic zone and the magmatic evolution in northern Ecuador [*Gutscher et al.*, 1999a; *Bourdon et al.*, 2003] suggest that slab flattening is active but not achieved, because the subduction of the Carnegie Ridge would be too recent. The Iquique Ridge may also be associated with a steep subducting slab below northern Chile because its subduction only began ~2 Ma ago [*Rosenbaum et al.*, 2005] (Figure 1c).

[30] The comparison between experiments 4 and 8 shows that the amount of subducted plateau when flat subduction initiates is similar (~11 cm) despite different convergence velocities (Figure 11). These experiments are scaled to represent the subduction of a 50-Ma-old oceanic plate overlain by a ~2-km-high plateau (Table 2), and the flat subduction occurs following the equivalent of ~700 km of plateau subduction (Figure 11). Part of the oceanic plateau is incorporated in the lower steep slab segment, and the flat slab segment is always much shorter than the amount of subducted plateau (Figures 5a and 9a). Numerical experiments of *Hassani et al.* [1997] also show that the slab flattening only starts when a sufficient length of buoyant slab is engaged in the subduction process despite the fact that their models do not incorporate preexisting dense subducting slab.

[31] These experimental results are consistent with the subducted length of the Nazca Ridge below Peru. In fact, the paleomagnetic reconstruction of the Nazca Ridge subduction shows that the subducted length of the Nazca Ridge below South America is ~900 km [*Hampel*, 2002]. The flat slab segment being ~700 km long, ~200 km of ridge are located in the steep part of the slab, as observed in experiments 4 and 8 (Figures 4a and 9a).

4.3. Deformation of the Overriding Plate

[32] Our models offer the possibility to study relationships between the subducting plate buoyancy and the related overriding plate deformation (Figure 12). When the trenchward overriding plate velocity is equal to the spontaneous trench retreat velocity, the overriding plate does not deform (experiments 1 and 4). The overriding plate shortens when kinematic boundary conditions impose larger convergence velocities and when buoyant plateaus are forced to subduct (experiments 4 and 8). This agrees with the numerical results by *Buiter et al.* [2001] and *Hampel and Pfiffner* [2006].
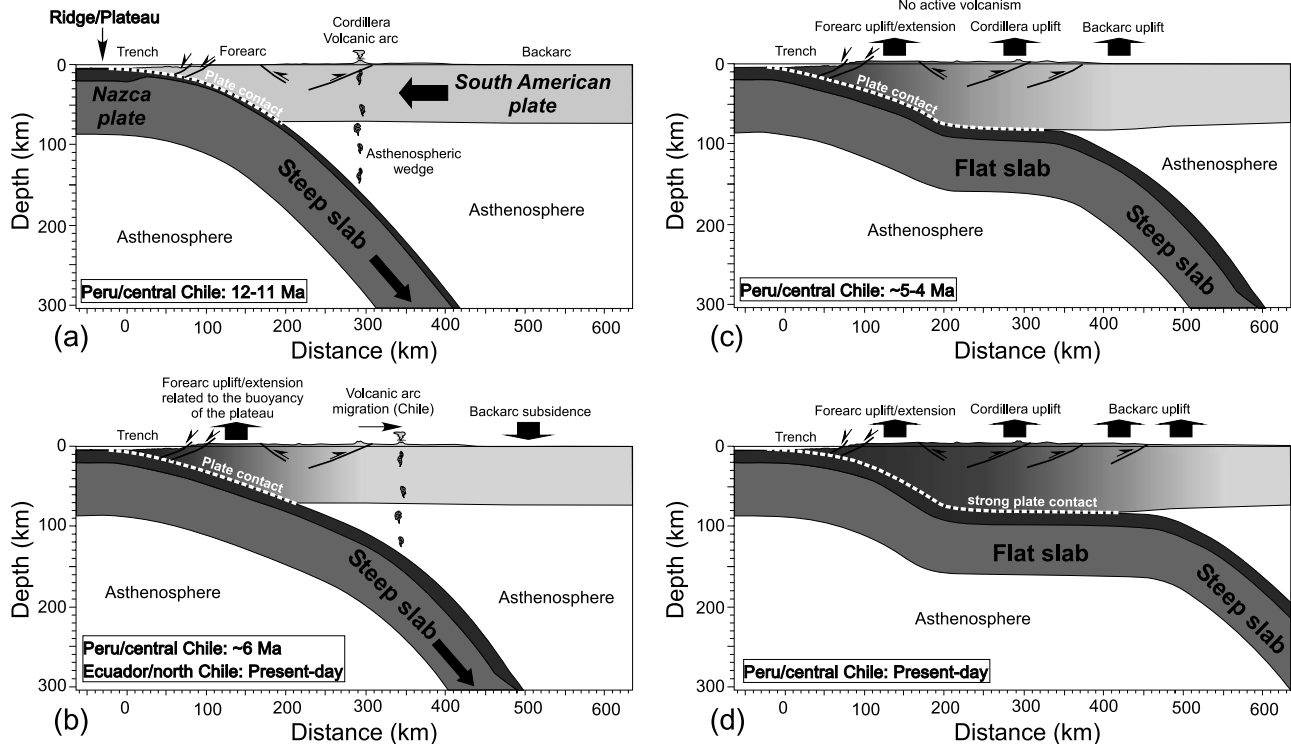
Figure 12. Schematic sketches showing evolution of the flat slab subduction process illustrated by analog models, applied to the Andean subduction zone (modified after *Gutscher et al.* [2000a]). (a) Steep subduction (>30° dip) during the subduction of the dense Nazca plate. (b) Subduction of buoyant and overthickened oceanic crust (e.g., ridge or oceanic plateau) with uplift of the fore-arc area. The buoyant slab is forced into subduction by the trenchward motion of the overriding plate. The dip of the slab decreases, and the volcanism migrates landward. (c) The upper slab starts to underplate the overriding plate, while the lower slab is steeper. Experiments suggest that it is necessary to involve a large amount of buoyant plate to obtain a flat slab segment, since part of the buoyant plateau is incorporated in the steep part of the slab to balance the negative buoyancy of the dense oceanic lithosphere. The strong plate contact is translated by the increase of the overriding plate shortening. The flat slab process cancels the vertical component of the slab favoring the uplift of the overriding plate. (d) Propagation of the flat slab segment beneath the overriding plate. The horizontal and buoyancy forces transmitted to the back-arc region cause back arc thrusting and uplift far from the trench.

[33] The topographic data presented here are purely qualitative. The effects of erosion and sedimentation have not been considered. Experiment 4 shows that the subduction of a plateau does not increase immediately the overriding plate shortening rate because plateau subduction does not result immediately in a decrease of the slab pull force (Figure 5d). In contrast, close to the trench, the overriding plate topography uplifts as soon as the plateau enters in the subduction zone (Figure 8a). This is interpreted as an isostatic adjustment accommodating the subduction of the plateau [*Moretti and Ngokwey*, 1985], while the slowly growing long-term uplift observed in the topographic high developing close to the trench results from overriding plate thickening (Figure 8b). The shortening rate in the overriding plate also increases following the appearance of the flat slab segment (Figure 4d). Cross sections demonstrate that overriding plate thickens and uplifts far from the trench, in the back-arc region, because the longer contact increases friction forces between plates (Figures 7 and 8). Consequently,

horizontal forces transmitted to the back-arc region may activate inherited weak zones and cause back arc thrusting in natural cases.

[34] These experimental results show that the flat subduction process induces a widespread shortening and uplift in the overriding plate, which is consistent with geological observations along the Andean subduction zone. The Ecuadorian fore arc exhibits Pliocene to Pleistocene marine terraces (so-called tablazos), which are exposed at 200–300 m above the Carnegie Ridge [*De Vries*, 1988; *Deniaud et al.*, 1999; *Pedoja et al.*, 2006]. *Gutscher et al.* [1999a] also show that the Carnegie Ridge is linked to a regional uplift of the fore arc more than 110 km landward. The subduction of the Carnegie Ridge is uplifting the coastal area, even if the flat subduction process is not achieved (Figure 12b). In Peru, the southward migration of the Nazca Ridge between 11 and 17°S has strongly influenced the geomorphology and tectonic activity of the Peruvian fore arc system [*Sébrier et al.*, 1985; *Hsu*, 1992; *Macharé and*

Table 2. Scaling of Parameters for the Reference Experiment (Experiment 1) (Table 3)

Parameter	Meaning	Unit	Model	Nature
g	gravitational acceleration	m s^{-2}	9.81	9.81
Thicknesses				
h	silicone/lithospheric plates	m	0.013	80,000
H	glucose syrup/upper mantle		0.10	660,000
	length scale factor $L_{\mathrm{Model}}/_{\mathrm{Nature}} = 1.5 \times 10^{-7}$			
Buoyancies				
$\Delta\rho_d = \rho_{gs} - \rho_d$	50-Ma-old oceanic lithosphere	kg m^{-3}	-80	-35
$\Delta\rho_p = \rho_{gs} - \rho_p$	50-Ma-old ocean, 1900-m-high plateau		$+41$	$+18$
$\Delta\rho_{op} = \rho_{gs} - \rho_{op}$	overriding plate		$+102$	$+45$
	buoyancy scale factor $\Delta\rho_{\mathrm{Model}}/\Delta\rho_{\mathrm{Nature}} = 2.3$			(normal continent: $+96$)
Viscosities				
η_d	dense subducting silicone/ 50-Ma-old oceanic lithosphere	Pa s	3.5×10^5	$\sim 10^{24}$
η_p	oceanic plateau		1.8×10^5	$\sim 10^{24}$
η_{op}	overriding lithosphere		1.6×10^5	$\sim 10^{23}$
η_{gs}	upper mantle		22	$\sim 10^{20}$
η_{lm}	lower mantle		∞	$\sim 10^{22}$
	viscosity scale factor $\eta_{\mathrm{Model}}/\eta_{\mathrm{Nature}} \sim 2 \times 10^{-19}$			
$t: (t_{\mathrm{Model}}/t_{\mathrm{Nature}}) = (\Delta\rho g L)_{\mathrm{Nature}}/ (\Delta\rho g L)_{\mathrm{Model}} \times (\eta_{\mathrm{Model}}/\eta_{\mathrm{Nature}}) = 1.3 \times 10^{-12}$	characteristic time	s	42 (42 s)	3.16×10^{13} (1 Ma)
$U: (U_{\mathrm{Model}}/U_{\mathrm{Nature}}) = (t_{\mathrm{Nature}} \times L_{\mathrm{Model}})/(t_{\mathrm{Model}} \times L_{\mathrm{Nature}}) = 1.1 \times 10^5$	characteristic velocity	m s^{-1}	3.3×10^{-4} (0.33 mm s^{-1})	2.9×10^{-9} (9.3 cm a^{-1})

Ortlieb, 1992; *Le Roux et al.*, 2000; *Hampel*, 2002; *Clift et al.*, 2003; *Hampel et al.*, 2004b; *Wipf*, 2006]. Pliocene to Pleistocene marine terraces developed above the Nazca Ridge indicate an uplift of ∼900 m of the coastal margin

[*Macharé and Ortlieb*, 1992]. In the Andes, the Nazca Ridge flat segment may control the shape of the modern topography of the cordillera. For example, the recent extensional collapse in the Cordillera Blanca [*McNulty*

Table 3. Experimental Parameters[a]

	Experiment							
	1	2	3	4	5	6	7	8
Width of the Plates (W)	0.305	0.2	0.3	0.305	0.3	0.3	0.3	0.3
Thickness of Silicone Plates (h)	0.013	0.012	0.013	0.013	0.013	0.012	0.013	0.013
Thickness of Glucose Syrup (H)	0.1	0.104	0.1	0.1	0.1	0.1	0.1	0.1
Piston Velocity	0	0	0	0.31	0.31	0.31	0.16	0.5
Dense Subducting Plate								
Length (L_d)	0.32	0.4	0.37	0.3	0.3	0.3	0.3	0.3
Density (ρ_d)	1496	1497	1496	1496	1496	1434	1434	1496
Viscosity (η_d)	3.5×10^5	2.7×10^5	3.5×10^5	3.5×10^5	3.5×10^5	3.5×10^5	3.5×10^5	3.5×10^5
Light Subducting Plate "Plateau"								
Length (L_p)	0.17	0.2	0.22	0.25	0.25	0.25	0.25	0.25
Density (ρ_p)	1375	1416	1375	1375	1375	1375	1375	1375
Viscosity (η_p)	1.8×10^5	2.6×10^5	1.8×10^5	1.8×10^5	1.8×10^5	1.8×10^5	1.8×10^5	1.8×10^5
Overriding Plate								
Length (L_{op})	0.225	-	-	0.18	0.19	0.2	0.2	0.15
Density (ρ_{op})	1314	-	-	1314	1314	1314	1314	1314
Viscosity (η_{op})	1.6×10^5	-	-	1.6×10^5	1.6×10^5	1.6×10^5	1.6×10^5	1.6×10^5
Glucose Syrup								
Density (ρ_{gs})	1416	1422	1416	1416	1416	1416	1416	1416
Viscosity (η_{gs})	22	12	22	22	22	22	22	22

[a]See also Figure 2 for the description of W, h, H, L_d, L_p, and L_{op}. Lengths are given in m, viscosities are given in Pa s, densities are given in kg m^{-3}, and velocities are given in mm s^{-1}. The evolutions of experiments 1, 4, and 8 are described in details in section 3. The results of experiments 2, 3, 5, 6, and 7 are used to build Figure 10.

and Farber, 2002] and Neogene counterclockwise rotations [*Rousse et al.*, 2003] would be related to the Nazca Ridge (Figure 12c). Similarly, the subduction of the Juan Fernandez Ridge below central Chile is marked by a Pliocene fore arc uplift [*Farias et al.*, 2008].

[35] In northern South America, part of the Amazonian basin located in front of the Peruvian flat slab segment displays deformation patterns related to the advance of the flat slab segment (Figures 1c and 12c) [*Dumont*, 1996; *Latrubesse and Rancy*, 2000; *Espurt et al.*, 2007]. This zone exhibits very wide sub-Andes, several uplifted basement blocks (Shira Mountains, Cushabatay High, and Moa Divisor range), and regional uplift (Fitzcarrald Arch uplift) above the eastern edge of the Nazca Ridge flat slab segment [*Espurt et al.*, 2007] (Figure 12d). Similarly, the eastward migration of the Juan Fernandez flat slab segment spatially coincides with the propagation of the deformation front of the precordillera thrust belt and the Pliocene uplift of the Sierras Pampeanas [*Allmendinger et al.*, 1983; *Ramos et al.*, 2002; *Giambiagi and Ramos*, 2002; *Siame et al.*, 2005] (Figure 12d). In addition, the subduction of the northern trench-parallel segment of the Juan Fernandez Ridge may explain the excess of 100 km of shortening exhibited by balanced cross sections during the Neogene to the north of the present-day flat slab segment [*Allmendinger et al.*, 1983; *Jordan and Alonso*, 1987; *Reynolds et al.*, 1990]. Similarly, *Rousse et al.* [2003] also suggest that the subduction of the northern segment of the Juan Fernandez Ridge during the Lower Miocene may explain the particularly intense shortening in the Bolivian Orocline at that time.

[36] We show that vertical displacements above the Andean flat slab segments are essentially deciphered in the fore-arc and back-arc regions. In fact, models suggest that vertical topographic motions related to the flat slabs would be observed in the entire of the Andean Cordillera, if we could eliminate the mountain-building processes.

[37] Finally, experiments suggest that the flat subduction, increasing the friction force between plates, may result in a decrease of the subduction velocity. This phenomenon is not clearly observed here because the boundary conditions we apply are purely kinematic and because in these experiments, the length of the superficial part of both plates is small when the flat slab segment occurs. *Gutscher et al.* [2000b] note that the seismic energy released within South America is 3–5 times larger above flat slab segments than above normal inclined segments. Seismicity clusters observed in the overriding plate of Peru and Argentina, east of the flat slab segments, are consistent with both the greater contact and friction between plates (Figures 1c and 12d) [*Gutscher et al.*, 2000b]. Thus the formation of two major flat slab segments during the Pliocene below the South American plate may explain the decrease of the eastward velocity of the Nazca plate during the last ~5 Ma [e.g., *Pardo-Casas and Molnar*, 1987; *Somoza*, 1998; *Norabuena et al.*, 1999]. This decreasing velocity has been attributed by *Iaffaldano et al.* [2006] to the uplift of the Altiplano Plateau, the load of which would consume a significant amount of the driving force responsible for the trenchward motion of the Nazca plate. In fact, the experiments show that flat slab segments also increase friction between plates, and the plot of the Nazca-Farallon/South America relative motion indicates two periods of slow convergence rates: one in the Oligocene between 35 and 26 Ma and the other one in the last 10 Ma [*Pardo-Casas and Molnar*, 1987]. These two periods are marked by the formation of large flat slab segments, below southern Peru and northern Chile in the Oligocene [*James and Sacks*, 1999] and below Peru and central Chile/NW Argentina from the Pliocene, suggesting a significant effect of the formation of flat segments on the subduction velocity.

5. Conclusions

[38] Lithospheric-scale analog experiments suggest that the appearance of flat slab segments can result only from large buoyant ridges/plateaus forced to subduct by the trenchward advance of the overriding plate, as previously suggested by *Gutscher et al.* [2000b] and *van Hunen et al.* [2002a, 2002b]. As a matter of fact, when negatively buoyant slab segments subduct below a trenchward advancing overriding plate, our experiments suggest that the overriding plate motion does not modify the vertical component of the slab velocity. Then, although increasing the overriding plate's trenchward motion results in a decrease of the dip of the slab, it is unable to create flat slabs, as observed below Peru and central Chile/NW Argentina.

[39] In our experiments modeling the subduction of a ~2-km-high plateau on a 50-Ma-old oceanic lithosphere, flat subduction only occurs after ~700 km of buoyant plateau subduction because part of the plateau is incorporated in the steep part of the slab to balance the negative buoyancy of the dense underlying oceanic slab. Hence the delay between the plateau subduction and the flattening of the slab is controlled by the trenchward velocity of the overriding plate.

[40] In South America, the Peruvian flat slab segments occurred ~7 Ma, following the beginning of the Nazca Ridge-Inca Plateau subduction. The same delay is observed between the subduction of the Juan Fernandez Ridge and the appearance of flat subduction below central Chile/NW Argentina. In northern Ecuador and northern Chile, the process of the slab flattening could be active but not completed, supporting the idea that the slab flattening needs time to occur.

[41] The overriding plate shortening rate increases following the subduction of an oceanic plateau as a result of the smaller slab pull force. In addition, it increases following the appearance of the flat slab because of a larger interplate friction force. The locus of maximum shortening migrates within the interior of the overriding plate when the slab flattens.

[42] The overriding plate topography close to the trench is immediately affected by the subduction of a buoyant plateau. We observe that two processes control the elevation of the overriding plate close to the active margin: (1) isostatic adjustments resulting in rapid topographic changes, depending on the buoyancy of the subducting plate at trench, and (2) overriding plate thickening. Finally, the appearance of

two major flat slab segments below South America ∼5 Ma ago may thus explain the decrease of the convergence velocity between the Nazca plate and the South American plate since that time.

References

Allmendinger, R. W., V. A. Ramos, T. E. Jordan, M. Palma, and B. L. Isacks (1983), Paleogeography and Andean structural geometry, northwest Argentina, *Tectonics*, *2*, 1–16, doi:10.1029/TC002i001p00001.

Baranzangi, M., and B. L. Isacks (1979), Subduction of the Nazca plate beneath Peru: Evidence from spatial distribution of earthquakes, *Geophys. J. R. Astron. Soc.*, *57*, 537–555.

Bellahsen, N., C. Faccenna, F. Funiciello, J. M. Daniel, and L. Jolivet (2003), Why did Arabia separate from Africa? Insights from 3-D laboratory experiments, *Earth Planet. Sci. Lett.*, *216*, 365–381, doi:10.1016/S0012-821X(03)00516-8.

Bourdon, E., J. P. Eissen, M.-A. Gutscher, M. Monzier, M. L. Hall, and J. Cotten (2003), Magmatic response to early aseismic ridge subduction: The Ecuadorian margin case (South America), *Earth Planet. Sci. Lett.*, *205*, 123–138, doi:10.1016/S0012-821X(02)01024-5.

Buiter, S. J. H., R. Govers, and M. J. R. Wortel (2001), A modelling study of vertical surface displacements at convergent plate margins, *Geophys. J. Int.*, *147*, 415–427, doi:10.1046/j.1365-246X.2001.00545.x.

Cahill, T., and B. L. Isacks (1992), Seismicity and shape of the subducted Nazca plate, *J. Geophys. Res.*, *97*, 17,503–17,529, doi:10.1029/92JB00493.

Chemenda, A. I., J. P. Burg, and M. Mattauer (2000), Evolutionary model of the Himalaya-Tibet system: Geopoem based on new modelling, geological and geophysical data, *Earth Planet. Sci. Lett.*, *174*, 397–409, doi:10.1016/S0012-821X(99)00277-0.

Chung, W. Y., and H. A. Kanamori (1978), Mechanical model for plate deformation associated with aseismic ridge subduction in New Hebrides Arc, *Tectonophysics*, *50*, 20–40.

Clift, P. D., I. Pecher, N. Kukowski, and A. Hampel (2003), Tectonic erosion of the Peruvian forearc, Lima Basin, by subduction and Nazca Ridge collision, *Tectonics*, *22*(3), 1023, doi:10.1029/2002TC001386.

Cloos, M. (1993), Lithospheric buoyancy and collisional orogenesis-subduction of oceanic plateaus, continental margins, island arcs, spreading ridges, and seamount, *Geol. Soc. Am. Bull.*, *105*, 715–737, doi:10.1130/0016-7606(1993)105<0715:LBACOS>2.3.CO;2.

Collot, J. Y., J. Daniel, and R. V. Burne (1985), Recent tectonics associated with the subduction/collision of the Entrecasteaux zone in the central New Hebrides, *Tectonophysics*, *112*, 325–356, doi:10.1016/0040-1951(85)90185-4.

Conrad, C. P., S. Bielk, and C. Lithgow-Bertelloni (2004), Great earthquakes and slab pull: Interaction between seismic coupling and plate-slab coupling, *Earth Planet. Sci. Lett.*, *218*, 109–122, doi:10.1016/S0012-821X(03)00643-5.

Dalmayrac, B., and P. Molnar (1981), Parallel thrust and normal faulting in Peru and constraints on the state of stress, *Earth Planet. Sci. Lett.*, *55*, 473–481, doi:10.1016/0012-821X(81)90174-6.

Davy, P., and P. R. Cobbold (1991), Experiments on shortening of a 4-layer continental lithosphere, *Tectonophysics*, *188*, 1–25, doi:10.1016/0040-1951(91)90311-F.

Deniaud, Y., P. Baby, C. Basile, M. Ordoñez, G. Montenegro, and G. Mascle (1999), Ouverture et évolution tectono-sédimentaire du golfe de Guayaquil: Bassin d'avant-arc néogène et quaternaire du sud des Andes équatoriennes, *C. R. Acad. Sci. Ser. 2*, *328*, 181–187.

DeVries, T. J. (1988), The geology of late Cenozoic marine terraces (tablazos) in northwestern Peru, *J. South Am. Earth Sci.*, *1*, 121–136, doi:10.1016/0895-9811(88)90030-2.

Dominguez, S., S. E. Lallemand, J. Malavieille, and R. von Huene (1998), Upper plate deformation associated with seamount subduction, *Tectonophysics*, *293*, 207–224, doi:10.1016/S0040-1951(98)00086-9.

Dumont, J. F. (1996), Neotectonics of the Subandes-Brazilian craton boundary using geomorphological data: The Marañon and Beni basins, *Tectonophysics*, *259*, 137–151, doi:10.1016/0040-1951(95)00200-6.

Engdahl, E. R., R. D. van der Hilst, and R. Buland (1998), Global teleseismic earthquake relocation with improved travel times and procedures for depth determination, *Bull. Seismol. Soc. Am.*, *88*, 722–743.

Espurt, N., P. Baby, S. Brusset, M. Roddaz, W. Hermoza, V. Regard, P.-O. Antoine, R. Salas-Gismondi, and R. Bolaños (2007), How does the Nazca Ridge subduction influence the modern Amazonian foreland basin?, *Geology*, *35*, 515–518, doi:10.1130/G23237A.1.

Farias, M., R. Charrier, S. Carretier, J. Martinod, A. Fock, D. Campbell, J. Caceres, and D. Comte (2008), Late Miocene high and rapid surface uplift and its erosional response in the Andes of central Chile (33°–35°S), *Tectonics*, *27*, TC1005, doi:10.1029/2006TC002046.

Funiciello, F., C. Faccenna, D. Giardini, and K. Regenauer-Lieb (2003), Dynamics of retreating slabs: 2. Insights from three-dimensional laboratory experiments, *J. Geophys. Res.*, *108*(B4), 2207, doi:10.1029/2001JB000896.

Funiciello, F., C. Faccenna, and D. Giardini (2004), Role of lateral mantle flow in the evolution of subduction systems: Insights from laboratory experiments, *Geophys. J. Int.*, *157*, 1393–1406, doi:10.1111/j.1365-246X.2004.02313.x.

Geist, E. L., M. A. Fisher, and D. W. Scoll (1993), Large-scale deformation associated with ridge subduction, *Geophys. J. Int.*, *115*, 344–366, doi:10.1111/j.1365-246X.1993.tb01191.x.

Giambiagi, L. B., and V. A. Ramos (2002), Structural evolution of the Andes in a transitional zone between flat and normal subduction (33°30′–33°45′S), Argentina and Chile, *J. South Am. Earth Sci.*, *5*, 101–116, doi:10.1016/S0895-9811(02)00008-1.

Gripp, A. E., and R. G. Gordon (2002), Young tracks of hotspots and current plate velocities, *Geophys. J. Int.*, *150*, 321–361, doi:10.1046/j.1365-246X.2002.01627.x.

Guillier, B., J. L. Chatelain, E. Jaillard, H. Yepes, G. Poupinet, and J. F. Fels (2001), Seismological evidence on the geometry of the orogenic system in central-northern Ecuador (South America), *Geophys. Res. Lett.*, *28*, 3749–3752, doi:10.1029/2001GL013257.

Gutscher, M.-A. (2002), Andean subduction styles and their effect on thermal structure and interplate coupling, *J. South Am. Earth Sci.*, *15*, 3–10, doi:10.1016/S0895-9811(02)00002-0.

Gutscher, M.-A., J. Malavieille, S. Lallemand, and J. Y. Collot (1999a), Tectonic segmentation of the North Andean margin: Impact of the Carnegie Ridge collision, *Earth Planet. Sci. Lett.*, *168*, 255–270, doi:10.1016/S0012-821X(99)00060-6.

Gutscher, M.-A., J. L. Olivet, D. Aslanian, J. P. Eissen, and R. Maury (1999b), The "lost Inca Plateau": Cause of flat subduction beneath Peru?, *Earth Planet. Sci. Lett.*, *171*, 335–341, doi:10.1016/S0012-821X(99)00153-3.

Gutscher, M.-A., R. Maury, J. P. Eissen, and E. Bourdon (2000a), Can slab melting be caused by flat subduction?, *Geology*, *28*, 535–538, doi:10.1130/0091-7613(2000)28<535:CSMBCB>2.0.CO;2.

Gutscher, M.-A., W. Spakman, H. Bijwaard, and E. R. Engdahl (2000b), Geodynamics of flat subduction: Seismicity and tomographic constraints from the Andean margin, *Tectonics*, *19*, 814–833, doi:10.1029/1999TC001152.

Hampel, A. (2002), The migration history of the Nazca Ridge along the Peruvian active margin: A re-evaluation, *Earth Planet. Sci. Lett.*, *203*, 665–679, doi:10.1016/S0012-821X(02)00859-2.

Hampel, A., and A. Pfiffner (2006), Relative importance of trenchward upper plate motion and friction along the plate interface for the topographic evolution of subduction-related mountain belts, in *Analogue and Numerical Modelling of Crustal-Scale Processes*, edited by S. J. H. Buiter and G. Schreurs, *Spec. Publ. Geol. Soc. London*, *253*, 105-115.

Hampel, A., N. Kukowski, J. Bialas, C. Huebscher, and R. Heinbockel (2004a), Ridge subduction at an erosive margin: The collision zone of the Nazca Ridge in southern Peru, *J. Geophys. Res.*, *109*, B02101, doi:10.1029/2003JB002593.

Hampel, A., J. Adam, and N. Kukowski (2004b), Response of the tectonically erosive south Peruvian forearc to subduction of the Nazca Ridge: Analysis of three-dimensional analogue experiments, *Tectonics*, *23*, TC5003, doi:10.1029/2003TC001585.

Hassani, R., D. Jongmans, and J. Chery (1997), Study of plate deformation and stress in subduction processes using two-dimensional numerical models, *J. Geophys. Res.*, *102*, 17,951–17,965, doi:10.1029/97JB01354.

Heuret, A., F. Funiciello, C. Faccenna, and S. Lallemand (2007), Plate kinematics, slab shape and back-arc stress: A comparison between laboratory models and current subduction zones, *Earth Planet. Sci. Lett.*, *256*, 473–483, doi:10.1016/j.epsl.2007.02.004.

Hsu, J. T. (1992), Quaternary uplift of the Peruvian coast related to the subduction of the Nazca Ridge: 13.5 to 15.6 degrees south latitude, *Quaternary Int.*, *15–16*, 87–97, doi:10.1016/1040-6182(92)90038-4.

Iaffaldano, G., H.-P. Bunge, and T. H. Dixon (2006), Feedback between mountain belt growth and plate convergence, *Geology*, *34*, 893–896, doi:10.1130/G22661.1.

James, D. E., and I. S. Sacks (1999), Cenozoic formation of the central Andes: A geophysical perspective, in *Geology and Ore Deposits of the Central Andes*, vol. 7, edited by B. J. Skinner, pp. 1–26, *Soc. Econ. Geol.*, Littleton, Colo.

Jarrard, R. D. (1986), Causes of compression and extension behind trenches, *Tectonophysics*, *132*, 89–102, doi:10.1016/0040-1951(86)90027-2.

Jordan, T. E., and R. W. Allmendinger (1986), The Sierras Pampeanas of Argentina: A modern analogue of Rocky Mountain foreland deformation, *Am. J. Sci.*, *286*, 737–764.

Jordan, T. E., and R. Alonso (1987), Cenozoic stratigraphy and basin tectonic of the Andes Mountains. 20°–28°, south latitude, *Am. Assoc. Pet. Geol. Bull.*, *71*, 49–56.

Kay, S. M., and C. Mpodozis (2002), Magmatism as a probe for the Neogene shallowing of the Nazca plate beneath the modern Chilean flat-slab, *J. South Am.Earth Sci.*, *15*, 39–57, doi:10.1016/S0895-9811(02)00005-6.

Kodama, K. (1984), A simple model calculation of the shear stress and surface profile caused by the perturbation on subducting plate, *J. Seismol. Soc. Jpn.*, *37*, 647–654.

Kopp, H., E. R. Flueh, C. Papenberg, and D. Klaeschen (2004), Seismic investigations of the O'Higgins Seamount Group and Juan Fernandez Ridge: Aseismic ridge emplacement and lithosphere hydration, *Tectonics*, *23*, TC2009, doi:10.1029/2003TC001590.

Latrubesse, E. M., and A. Rancy (2000), Neotectonic influence on tropical rivers of southwestern Amazon during the late Quaternary: The Moa and Ipixuna river basins, Brazil, *Quaternary Int.*, *72*, 67–72, doi:10.1016/S1040-6182(00)00022-7.

Le Roux, J. P., C. Tavares Correa, and F. Alayza (2000), Sedimentology of the Rimac-Chillon alluvial fan at Lima, Peru, as related to Plio-Pleistocene sea level changes, glacial cycles and tectonics, *J. South Am. Earth Sci.*, *13*, 499–510, doi:10.1016/S0895-9811(00)00044-4.

Lonsdale, P., and K. D. Klitgord (1978), Structure and tectonic history of the eastern Panama Basin, *Geol. Soc. Am. Bull.*, *89*, 981–999, doi:10.1130/0016-7606(1978)89<981:SATHOT>2.0.CO;2.

Macharé, J., and L. Ortlieb (1992), Plio-Quaternary vertical motions and the subduction of the Nazca Ridge, central coast of Peru, *Tectonophysics*, *205*, 97–108, doi:10.1016/0040-1951(92)90420-B.

Marrett, R., and M. R. Strecker (2000), Response of intracontinental deformation in the central Andes to late Cenozoic reorganization of South American plate motions, *Tectonics*, *19*, 452–467, doi:10.1029/1999TC001102.

Martinod, J., F. Funiciello, C. Faccenna, S. Labanieh, and V. Regard (2005), Dynamical effects of subducting ridges: Insights from 3-D laboratory models, *Geophys. J. Int.*, *163*, 1137–1150.

McGeary, S., A. Nur, and Z. Ben-Avraham (1985), Special gaps in arc volcanism: The effect of collision or subduction of oceanic plateaus, *Tectonophysics*, *119*, 195–221, doi:10.1016/0040-1951(85)90039-3.

McNulty, B., and D. Farber (2002), Active detachment faulting above the Peruvian flat slab, *Geology*, *30*, 567–570, doi:10.1130/0091-7613(2002)030<0567:ADFATP>2.0.CO;2.

Molnar, P., and D. Gray (1979), Subduction of continental lithosphere: Some constraints and uncertainties, *Geology*, *7*, 58–62, doi:10.1130/0091-7613(1979)7<58:SOCLSC>2.0.CO;2.

Moretti, I., and K. Ngokwey (1985), Aseismic ridge subduction and vertical motion of overriding plate, paper presented at the Symposium Paris, Géodynamique des Caraïbes, Paris, 5–8 Feb.

Norabuena, E. D., T. H. Dixon, S. Stein, and C. G. A. Harrison (1999), Decelerating Nazca-South America and Nazca-Pacific plate motions, *Geophys. Res. Lett.*, *26*, 3405–3408, doi:10.1029/1999GL005394.

Nur, A., and Z. Ben-Avraham (1981), Volcanic gaps and the consumption of aseismic ridges in *South America, in Nazca Plate: Crustal Formation and Andean Convergence*, edited by L. D. Kulm et al., *Mem. Geol. Soc. Am.*, *154*, 729-740.

Pardo, M., D. Comte, and T. Monfret (2002), Seismotectonic and stress distribution in the central Chile subduction zone, J. South Am, *Earth Sci.*, *15*, 11–22, doi:10.1016/S0895-9811(02)00003-2.

Pardo-Casas, F., and P. Molnar (1987), Relative motion of the Nazca (Farallón) and South America plate since late Cretaceous times, *Tectonics*, *6*, 233–248, doi:10.1029/TC006i003p00233.

Pedoja, K., J. F. Dumont, M. Lamothe, L. Ortlieb, J.-Y. Collot, B. Ghaleb, M. Auclair, V. Alvarez, and B. Labrousse (2006), Plio-Quaternary uplift of the Manta Peninsula and La Plata Island and the subduction of the Carnegie Ridge, central coast of Ecuador, *J. South Am. Earth Sci.*, *22*, 1–21, doi:10.1016/j.jsames.2006.08.003.

Pilger, R. H. (1981), Plate reconstructions, aseismic ridges, and low-angle subduction beneath the Andes, *Geol. Soc. Am. Bull.*, *92*, 448–456, doi:10.1130/0016-7606(1981)92<448:PRARAL>2.0.CO;2.

Ramos, V. A., E. O. Cristallini, and D. J. Pérez (2002), The Pampean flat-slab of the central Andes, *J. South Am. Earth Sci.*, *15*, 59–78, doi:10.1016/S0895-9811(02)00006-8.

Regard, V., C. Faccenna, J. Martinod, and O. Bellier (2005), Slab pull and indentation tectonics: Insights from 3D laboratory experiments, *Phys. Earth Planet. Inter.*, *149*, 99–113, doi:10.1016/j.pepi.2004.08.011.

Reynolds, J. H., T. E. Jordan, N. M. Johnson, J. F. Damanti, and K. D. Tabbutt (1990), Neogene deformation of the flat-subduction segment of the Argentine-Chilean Andes: Magnetostratigraphic constraints from Las Juntas, La Rioja province, Argentina, *Geology*, *102*, 1607–1622.

Rosenbaum, G., D. Giles, M. Saxon, P. G. Betts, R. F. Weinberg, and C. Duboz (2005), Subduction of the Nazca Ridge and the Inca Plateau: Insights into the formation of ore deposits in Peru, *Earth Planet. Sci. Lett.*, *239*, 18–32, doi:10.1016/j.epsl.2005.08.003.

Rousse, S., S. Gilder, D. Farber, B. McNulty, P. Patriat, V. Torres, and T. Sempere (2003), Paleomagnetic tracking of mountain building in the Peruvian Andes since 10 Ma, *Tectonics*, *22*(5), 1048, doi:10.1029/2003TC001508.

Sacks, I. S., and H. Okada (1974), A comparison of the anelasticity structure beneath western South America and Japan, *Phys. Earth Planet. Inter.*, *9*, 211–219, doi:10.1016/0031-9201(74)90139-3.

Sallarès, V., P. Charvis, E. R. Flueh, and J. Bialas (2005), Seismic structure of the Carnegie ridge and the nature of the Galápagos hotspot, *Geophys. J. Int.*, *161*, 763–788, doi:10.1111/j.1365-246X.2005.02592.x.

Scholz, C. H., and J. Campos (1995), On the mechanism of seismic decoupling and back-arc spreading at subduction zones, *J. Geophys. Res.*, *100*, 22,103–22,115, doi:10.1029/95JB01869.

Sébrier, M., J. L. Mercier, F. Mégard, B. Laubacher, and E. Carey-Gailhardis (1985), Quaternary normal and reverse faulting and the state of stress in the central Andes of south Peru, *Tectonics*, *4*, 739–780, doi:10.1029/TC004i007p00739.

Siame, L. L., O. Bellier, M. Sébrier, and M. Araujo (2005), Deformation partitioning in flat subduction setting: Case of the Andean foreland of western Argentina (28°S–33°S), *Tectonics*, *24*, TC5003, doi:10.1029/2005TC001787.

Silver, P. G., R. M. Russo, and C. Lithgow-Bertelloni (1998), Coupling of South American and African plate motion and plate deformation, *Sciences N. Y.*, *279*, 60–63.

Smith, H. F. W., and D. T. Sandwell (1997), Global seafloor topography from satellite altimetry and ship depth soundings, *Science*, *277*, 1956–1961, doi:10.1126/science.277.5334.1956.

Soler, P., M. G. Bonhomme (1990), Relation of magmatic activity to plate dynamics in central Peru from Cretaceous to present, in *Plutonism From Antarctica to Alaska*, edited by S. M. Kay and C. W. Rapela, *Geol. Soc. Am. Spec. Pap.*, *241*, 173-192.

Somoza, R. (1998), Updated Nazca (Farallon)-South America relative motions during the last 40 My: Implications for mountain building in the central Andean region, *J. South Am. Earth Sci.*, *11*, 211–215, doi:10.1016/S0895-9811(98)00012-1.

Spikings, R. A., W. Winkler, D. Seward, and R. Handler (2001), Along-strike variations in the thermal and tectonic response of the continental Ecuadorian Andes to the collision with heterogeneous oceanic crust, *Earth Planet.Sci. Lett.*, *186*, 57–73, doi:10.1016/S0012-821X(01)00225-4.

Tassara, A., H.-J. Götze, S. Schmidt, and R. Hackney (2006), Three-dimensional density model of the Nazca plate and the Andean continental margin, *J. Geophys. Res.*, *111*, B09404, doi:10.1029/2005JB003976.

van Hunen, J., A. P. van den Berg, and N. J. Vlaar (2002a), On the role of subducting oceanic plateaus in the development of shallow flat subduction, *Tectonophysics*, *352*, 317–333, doi:10.1016/S0040-1951(02)00263-9.

van Hunen, J., A. P. van den Berg, and N. J. Vlaar (2002b), The impact of the South American plate motion and the Nazca Ridge subduction on the flat subduction below South Peru, *Geophys. Res. Lett.*, *29*(14), 1690, doi:10.1029/2001GL014004.

van Hunen, J., A. P. van den Berg, and N. J. Vlaar (2004), Various mechanisms to induce present-day shallow flat subduction and implications for the younger Earth: A numerical parameter study, *Phys. Earth Planet. Inter.*, *146*, 179–194, doi:10.1016/j.pepi.2003.07.027.

Vlaar, N. J. (1983), Thermal anomalies and magmatism due to lithospheric doubling and shifting, *Earth Planet. Sci. Lett.*, *65*, 322–330, doi:10.1016/0012-821X(83)90170-X.

von Huene, R., I. Pecher, and M.-A. Gutscher (1996), Development of the accretionary prism along Peru and material flux after subduction of Nazca Ridge, *Tectonics*, *15*, 19–33, doi:10.1029/95TC02618.

Wagner, L. S., S. Beck, and G. Zandt (2005), Upper mantle structure in the south central Chilian subduction zone (30° to 36°S), *J. Geophys. Res.*, *110*, B01308, doi:10.1029/2004JB003238.

Weijermars, R., and H. Schmeling (1986), Scaling of Newtonian and non-Newtonian fluid dynamics without inertia for quantitative modelling of rock flow due to gravity (including the concept of rheological similarity), *Phys. Earth Planet. Inter.*, *43*, 316–330.

Wipf, M. A. (2006), Evolution of the Western Cordillera and coastal margin of Peru: Evidence from low-temperature thermochronology and geomorphology, Ph.D. thesis, Swiss Fed. Inst. of Technol., Zürich, Zürich, Switzerland.

Woods, M. T., and E. A. Okal (1994), The structure of the Nazca Ridge and Sala y Gomez seamount chain from dispersion of Rayleigh waves, *Geophys. J. Int.*, *117*, 205–222, doi:10.1111/j.1365-246X.1994.tb03313.x.

Wortel, M. J. R., and W. Spakman (2000), Subduction and slab detachment in the Mediterranean-Carpathian region, *Science*, *290*, 1910–1917, doi:10.1126/science.290.5498.1910..

Yáñez, G. A., C. R. Ranero, R. von Huene, and J. Díaz (2001), Magnetic anomaly interpretation across the southern central Andes (32°–34°S): The role of the Juan Fernández Ridge in the late Tertiary evolution of the margin, *J. Geophys. Res.*, *106*, 6325–6345, doi:10.1029/2000JB900337.

S. Brusset, B. Guillaume, J. Martinod, and V. Regard, Laboratoire des Mécanismes et Transferts et Géologie, Université de Toulouse, CNRS, IRD, OMP, 14 Avenue E. Belin, F-31400 Toulouse, France.

N. Espurt, Institut Français du Pétrole, 1 et 4 Avenue de Bois-Préau, F-92852 Rueil-Malmaison Cedex, France. (espurt@lmtg.obs-mip.fr)

C. Faccenna and F. Funiciello, Dipartimento Scienze Geologiche, University Roma TRE, L. S. Leonardo Murialdo 1, I-00146 Rome, Italy.